UNIVERSITY OF LEEDS

Aircraft Landing Gear

Mini Project- Group Report

M Harmon, M Mesaritis, J Makin, N Salman, L Wechie

December 2014

Professor R Dwyer-Joyce

ABSTRACT

The design and selection of bushes for landing gears is a very important application in engineering. This report aims to shed light on the materials that could be used and their testing procedures. This report surveys and evaluates the use of self-lubricating bearing materials for bushes in aircraft landing gear as opposed to lubricated bearings. Three commercially important lubricating materials have been investigated in much greater detail, the materials in question are; Aluminium Bronze, Beryllium Copper and ToughMet. Simultaneously, a test rig to determine the wear properties of the surveyed materials was designed. Two predictive wear models, capable of predicting the wear on a bearing via two separate wear modes, both linked intrinsically to the motion experienced in landing gear have been proposed. Finally, testing was completed to determine the effect of contaminants on material properties.

NOMENCLATURE

μ	Coefficient of Friction
D	Sliding Distance (m)
d	Bearing Diameter
F	Applied Load (N)
k	Wear Coefficient (m^2N^{-1})
L	Bearing Width
P	Contact Pressure
r	Shaft Radius (m)
T	Torque (Nm)
V	Wear Volume (m^3)
Fp	Normal Load on the bearing (N)
Rb	Bearing radius (m)
Rs	Shaft radius (m)
F_N	Normal Reaction force of the bearing (N)
F_F	Tangential Reaction force of the bearing (N)
α	Bearing Angle (deg)
d	Bearing diameter (m)
ω	Rotational speed (rad/s)
b	Half width of contact (m)
R	Curvature Sum
E'	Equivalent Modulus (GPa)
E_1	Elastic modulus of shaft (GPa)
E_2	Ealstic modulus of bearing (GPa)
υ_1	Poisson's ratio of shaft
υ_2	Poisson's ratio of bearing

W	Normal force (N)
D	Sliding Distance (m)
C	Number of cycles
P_{max}	Maximum pressure (GPa)
P_{Mean}	Mean Pressure (GPa)
ε	Strain
σ	Stress (Pa)
P_i	Pressure at node position i
y	Distance from centreline

CONTENTS

TABLE OF FIGURES

ACKNOWLEDGEMENTS

We would like to thank Professor Rob Dwyer-Joyce for his support throughout this project. We would also like to thank Alex Baker for his help with the contaminant sample testing and Pete Krier for help on the rig design and wear modelling.

1 PROBLEM STATEMENT

The landing gear of an aircraft consists of a lot of pin joints allowing the structure to articulate and these joints contain a lot of bushes made of aluminium bronze, which are all lubricated with grease. An A320 landing gear consists of thirty two joints and three hundred greasing points. Since the process of greasing is time consuming and costly, as well as the fact that it is not weigh efficient, the solution is to use self-lubricating bushes instead of the metal ones.

2 OBJECTIVES

- Examine the properties of bearing materials
- Determine the commercial self-lubricating bearing materials available.
- Investigate the commercial self-lubricating bearing materials, classify them and compare their properties by plotting their PV and other graphs.
- Investigate the three bearing materials; Aluminium Bronze, Beryllium Copper and ToughMet.
- Present the excel sheet for material selection.
- Develop a test machine capable to examine the tribological behaviour of self-lubricating bearings.
- The bearings must be tested under several conditions and in a combination of reciprocating angular movement and continuous movement.
- Develop predictive wear model for two different modes of wear
- Investigate different materials with contamination typically used in landing gears system.

3 INTRODUCTION

3.1 Landing Gear Pin Joints

The landing gears are major components in aircrafts because they are the main parts carrying the load and supporting the aircraft. The landing gear is used to support the aircraft on the ground, which allows it to taxi but most importantly to take-off and land. They need to be designed with minimum weight, high performance and life time, taking into consideration the need to absorb the landing impact loads, strength requirements, damping, stability, as well as other requirements (Zhu et al. 2012). The landing gear also has the break and wheel steering systems.

The extending and retracting of the landing gear is done by an articulating structure which uses many pin joints to allow mechanical articulation. These pin joints are made of steel and it reciprocates inside a bush as shown in Figure 3.1.1. These bushes are usually made of aluminum bronze and the pin joints are all grease lubricated. The main landing gear of an aircraft usually consists of many pin joints and they have many greasing points. These greasing points are manually fed on a specific maintenance timetable, this seems to be a good solution tribologically to provide a suitable bearing surface, however it increases the weight of the landing gear, it is time consuming and costly. Thus, a solution for that is to use dry rubbing self-lubricating bushes or plain bearings that do not need lubrication and are maintenance free.

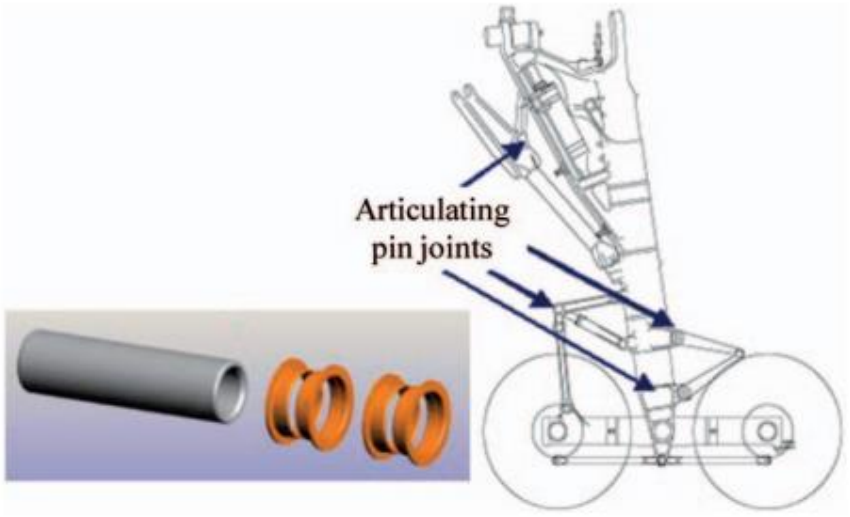

Figure 3.1.1: Illustrative Sketch of a Landing Gear, Pint Joint and Bushes (Zhu, et al., 2012)

These plain bearings have to be made of durable materials with high wear resistance, low friction, resistance to high temperatures and also have to be corrosion resistant (Shvedkov 1983). Generally, bearings running with lubrication have drawbacks and are totally unsuitable

for some operations, and in these cases only self-lubricating bearings could be used, which are made using powder metallurgy and that is why 78% of the United States and 66% of Japan's powder productions are used in the manufacturing of these plain bearings.

3.2 **Dry Rubbing Self-Lubricating Bearing Materials**

A self-lubricating material is a material that is able to slide against a metal counter surface; mostly steels, at appropriate loads and speeds without the use of a lubricant and without suffering the damages which would normally occur if metal surfaces rub together without lubrication, hence it is called dry rubbing (Evans & Senior 1982). A plain bearing is one where the predominant motion is sliding, typically a plain bearing, a bush or thrust washer.

Material elements used to make self-lubricated dry rubbing materials, are with weak bonds not strong ones, because bonding can be strong at contact points and sever surface damage and failure can occur, so weak adhesion between components is needed and thus the more the inhomogeneous of the material structure, the less likely it will grow areas of adhesion (Kozma 2001). The most common way is to use solid lubricants, by applying films to metallic surfaces. The solid can be a binder containing a liquid carrier and applying it as a film, it can be rubbed into the surface or vapour deposited (Fusaro 1990). The other common way is to make the materials as a self-lubricating composite, which consists of a matrix reinforcement, a solid additive and other binding elements for stability.

It would sound easy to live up to the performance and life requirements of bearings, however when the operating conditions and the environment is considered, the matter becomes difficult. Those factors are usually many and they change all the time, and once they do, it is very hard to predict the performance and life, based on other bearings or test that has been done before. This is even truer for dry rubbing and thus selecting and qualifying self-lubricating bearings remains a difficult task in aircraft applications such as in the landing gears.

Little experience with the requirements of self-lubricating materials was found at the beginning of the upcoming of the aircraft or space industry (Christy 1982). Between the years 1959 and 1975, a lot of research was done on the requirements for dry lubricants because they were worried about cold welding and other possible failures, where a failure in lubricant could cause in the loss of an aircraft. It is still not possible to undertake a general research and testing to know the purpose of dry lubricants due to the vast range of applications and hence, researches always have a specific application in mind. That is also why in literature, papers

always start with the selection of the lubricant which is based on extreme testing under specific conditions.

Self-lubricating bearing materials meet a large number of strict requirements which are specified at the first instance by the operation conditions for their intended parts. Thus, a huge number of classifications of self-lubricating bearings exist and they do not have much in common. In our research we follow the classification scheme showed in Figure 3.2.1. This classification forms the basis of the survey done in this report on the commercial available self-lubricating bearing materials, as will be shown in latter chapters.

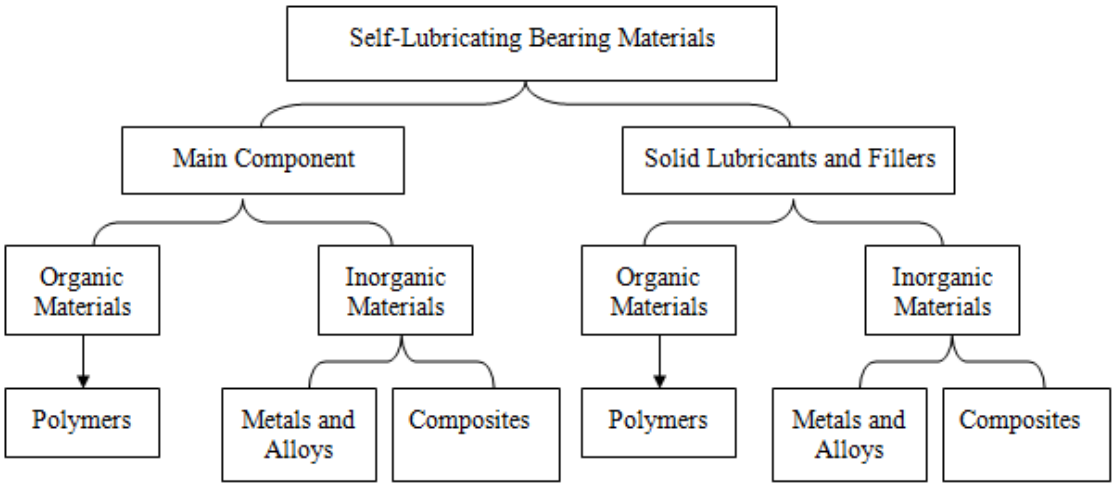

Figure 3.2.1: Classification of Self-Lubricating Bearing Materials

4 CATALOGUE OF MATERIALS

This part of the report investigates the bearing materials. First a background is given about the type of bearing materials used, the performance criteria and physical properties. After that, a detailed survey of the commercially available self-lubricating bearings is presented, as well as a comparison between the three lubricating bearing materials; Aluminium Bronze, Beryllium Copper and ToughMet Bearing Materials is conducted. Finally, the method for the material selection is shown.

4.1 Bearing Materials Properties

1.1.1. **Material type**

Depending on the application and working conditions, there is a wide range of materials to choose from when designing a bearing. The materials are processed and combined to increase the life of the bearing as much as possible as well as its performance. The following materials are used for self-lubricating applications with a focus on the aircraft industry and mainly its landing gears.

Self-lubricating bearings fall into three main categories as explained before:

- Metal and Alloy-based materials
- Polymer-based materials
- Composite materials

4.1.1.1 **Metal and Alloy-based Materials**

Metal based self-lubricating bearings usually contain in changing proportions Cu, Sn, Fe, Al and other metals, such as Ni, Pb,Zn and MoS, which are added to them. Graphite is also usually used due to its ability to greatly improve self-lubrication qualities. Porosity when using such materials ranges from 0-35% (Morgan 1979).

Due to its easy chemical and physical processing copper is one of the most commonly used self-lubricating bearings. As a matter of fact, copper is usually used as a base for these bearings. They are usually sintered with lead, tin or bronzes containing lead. Increasing porosity usually enables lead content to be raised up to 50%. Bronze compositions with 10-40% Pb or 1-10% Sn are commonly used (Pratt 1969). Replacing bronze with other materials didn't have any success previously, mainly due to the processing qualities of bronze which remain superior.

Copper based bearings may also use sulfides, especially MoS_2 and WS_2, usually done by Japanese companies where, Mn with 55-98% MoS_s is usually added to a copper based mixture. The operational conditions of metalloplastic bearings is usually up to PSP=140 MPa and up to pv=3.6 MPa.m/sec where the temperature ranges from -200 to +289°c (Shvedkov, 1983).

Steel based bearings may also be used for reciprocating motion conditions, where a load-carrying steel backing and sinter bonded with a porous bronze filled with ptfe. The composition of ptfe is usually 45-95% ptfe, 5-50%Zn, and 1-5% Al203. The previous bearing was designed by Kogyo k. k. a Japanese firm.

4.1.1.2 **Polymer-based Materials**

Polymer-based bearings are usually based on ptfe (Floroplast, Teflon) which is due to its superior combination of qualities when compared to other polymers. It is wildly used in airspace applications because it is chemically stable, has high plasticity and high anti-friction qualities and low sliding speed. The coefficient of friction is usually around 0.010 without lubrication (Brookes 1980). Since they are mostly used as bearing materials by themselves they are employed in marine applications with very large sizes.

However, as a standalone, ptfe has low strength and low load carrying capacity which may be unsatisfactory for certain applications. Therefore, fillers such as lead and other metals, alloys such as bronze, compounds such as sulfides and red lead oxide and other substances such as graphite are usually added (Pratt 1969).They may also be reinforced with carbon fibers or ceramic may be used as a fillin .

Other polymers may also be used as bearings whether thermoplastic or thermoset such as: nylon, polyethylene, polyacetal, phenol-formaldehyde, epoxy, and organosilicon resins. Polyacetal may also be used either by itself or by adding ptfe especially when using it in self-lubricating applications (Shvedkov 1983). It may also be reinforced with glass fibers. Polyamide with graphite is used in order to raise the operating temperatures to up to 260°c. This is usually found in rotary inlet guide vanes for airplanes.

4.1.1.3 **Composite Materials**

Reinforcements are usually done extensively using carbon; mainly graphite, fibers both plane and composite such as when using B or Ti coating (Eliezer et al. 1978). Polymers such as; polyformaldehyde, polyamide, phenol, and epoxy resins, nylon, polyphenylenesulfate, and others, as well as metals bearings mainly copper alloys are usually subject to such reinforcement of graphite (Pratt 1969). Reinforcing bronze with carbon fibres allowed it to operate at v=325 m/s.

Reinforcement is either done through continuous or chopped wires such as p.t.f.e 77.5% reinforced with asbestos 53 or graphite 5. Such reinforcement yields dimensional stability and good wear resistance.

In very sever conditions, materials filled with large particles of wear-resistant hard materials are becoming common practice. The matrix is usually a ductile material generally tin or lead bronzes, or copper or lead based alloys are all used. The reinforcement are usually granules of Srellite, Relit, Sormait or other hard metals. Sometimes intermetallic compounds such as TiAl maybe specifically tailored as a filler for copper alloy which have shown to reduce friction coefficient and wear of the bearing and the shaft.

Operating in temperatures between cryogenic and 480 degrees or higher, bearings with up to 20 vol% steel are introduced into an aluminium copper alloy matrix or the addition of Stellite to a bronze matrix which is used for sliding bearings in drilling mills (Shvedkov 1983).

1.1.2. **Performance Criteria**

Sliding bearings have two main property requirements:

- The material must be able to support the load applied in the conditions and environment concerned with deformation or loss in strength.
- The material much be of low coefficient of friction and ware rate, and preferably they will not change much by changing the operating conditions or the environments; such as conditions of sliding, temperature, contamination and humidity.

Therefore, the coming criteria are the main performance criteria that must be considered in designing or selecting a bearing material.

4.1.1.4 **Load Capacity**

The load carrying capacity cannot be defined based on a single strength parameter in dry bearing. Within contact areas, both tensile and compressive stresses occurs, as well as shear stresses in the layers of the material (Lancaster 1973). Mostly, the loading capacity is determined at one-third of the maximum compressive stress, however, that is only applicable for materials that have similar compressive and tensile properties.

Furthermore, some materials also have a visco-elastic behaviour where their properties depend on time. At any specific loading rate, the stress-strain relationships of a material are nonlinear, creep and plastic deformation can occur even under static loading. Therefore, it is not possible to specify the elastic moduli generally for many dry bearing materials. In most

applications that is not accounted as a problem because the stiffness of a dry bearing assembly is not an important parameter. However, in air-frame bearings, the stiffness is very important, where it is more appropriate to use tensile moduli acquires through conventional testing methods.

4.1.1.5 **Wear**

The wear of an object is associated with the removal and/or deformation of the surface material (Williams 2005) Material properties such as Hardness (H), Modulus of Elasticity (E) and Poisson's ratio (υ) contribute to the wear resistance of a material.

The wear of a component can be caused by a number of different mechanisms that do not necessarily act independently and are not mutually exclusive (Archard 1980). The two main causes of wear in dry rubbing bearings are adhesive wear and abrasive wear, often acting simultaneously (Williams 2005).

Adhesive wear occurs when two materials come under frictional contact. Adhesive wear begins when respective asperities on each counterface come into contact with one another and coalesce, further movement causes the connection between the two asperities to break, resulting in the removal of material causing wear debris (Stachowiak & Batchelor 2014b).

Abrasive wear occurs when a harder surface slides across a softer surface, this can be two-body or three-body wear. Two-body wear is when the asperities of the harder surface cause wear tracks in the softer surface, three-body wear occurs when wear debris has entered the system and 'ploughs' the softer surface (Stachowiak & Batchelor 2014a).

In the operation with of dry bearings wear is one of the greatest uncertainties. According to the simple theory, as well as experimental studies, once a steady-state of the surface conditions is attained during sliding, the wear volume v will be proportional to the siding distance d Archard (1986). Thus, if the load has no effect on any other variables, particularly the surface temperature, then the load is directly proportional to the wear per unit sliding distance as shown in Equation 4.1.1

$$v = kWD$$

Equation 4.1.1

Where k is the specific wear rate and is a material property however, it might depend on the geometry and sliding conditions, and hence the uncertainty.

4.1.1.6 **PV Factor**

The concept of PV, where P is the maximum loading capacity and V the sliding velocity, is directly related to the expression of the wear rate in terms of radial wear per time. The PV factors either takes a limiting form, as above, where wear increases rapidly due to temperature effects or elasticity, or it takes the form of a continuous operation at some specified wear rate (arbitrarily). The best criteria of performance in bearings is a PV curve at a specific wear rate. However, in both forms, the PV factor is not a unique criteria of performance due to the assumptions that P and V do not have an effects on other variables, which is not valid in most cases.

Figure 4.1.1 shows a typical PV curve for a constant wear rate, and it shows that P and V are inversely proportional in the central range of PV. However for low speeds, the strength of the material limits the maximum P that can be used, and as the maximum P is approached, the constant wear rate is no longer independent of load and starts to increase. At high speeds, the temperature of the surface increases due to friction and that leads to the increase in wear rate.

Due to this non-linearity in PV curves, it is best to express the design information of self-lubricating bearings with complete PV relations. However, no sufficient data is available for PV factors for commercially available materials, they only present information at one or two speeds at best.

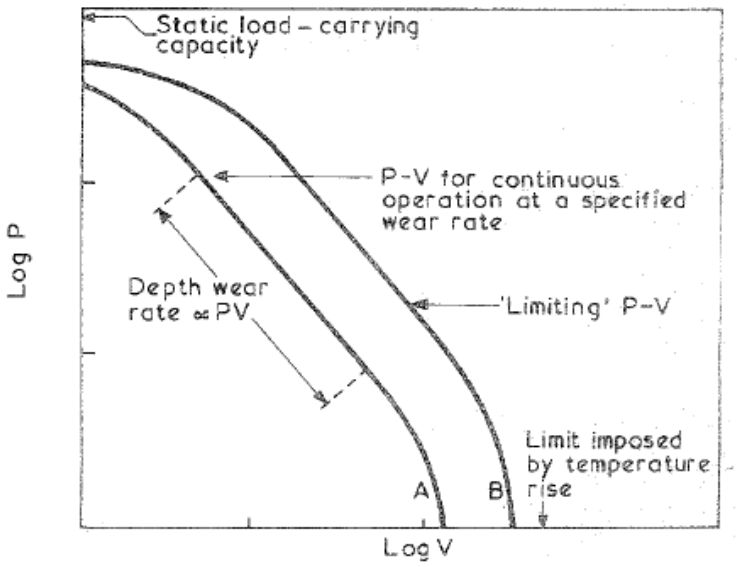

Figure 4.1.1: Relationships Between P and V for Dry Bearings (Lancaster 1973)

1.1.3. **Physical Properties**

There are also some physical properties that must be taken into consideration such as:

- Corrosion Resistance
- Melting Range
- Surface Hardness
- Coefficient of linear thermal expansion (10-6/K)
- Thermal Conductivity (W/m.K)
- Surface Roughness (μm)
- Weight

1.1.4. **Environmental Effects**

There are important environmental effects too, that could change and affect the material's properties such as:

- Radiation
- Vacuum
- Water
- Oils
- Abrasives
- pH

4.2 **Survey on Commercially Available Dry Rubbing Self-Lubricating Bearing Materials**

This section covers the survey and investigation of the commercially available self-lubricating bearing materials. The survey was done on different bearing materials made by different companies. An excel sheet was constructed to contain all these materials and their characteristics and properties.

Needless to say, bearings provide a relative movement between parts and the selection of the bearing is very crucial to retain performance and life requirements under the specific conditions and environment. The selection of the type and form of the bearing; whether it should be a plain, ball or spherical bearing or others, and their arrangements, all depends on the nature of that relative movement of the parts, as well as the constraints. In our case, in the pin joint of the main landing gear in the aircraft, a plain bearing is used as explained before.

However for the selection of the material, one should take into consideration the operation conditions and the surrounded environments, such as the magnitude and direction of the load, speed of sliding contacts, temperature, friction and others. Thus, here looking at the performance criteria of the materials is crucial and based on that the material is selected.

The excel sheet constructed provides a very easy and handy manual to select the self-lubricating bearing material needed for any specific condition based on their performance criteria. Most of the commercial self-lubricating bearing materials are included, as well as the three lubricating materials; Aluminium Bronze, Beryllium Copper and ToughMet which will be covered in the next section of the report.

The materials are categorized in the excel sheet according to material type as in Figure 3.2.1, as well as according to company, so it could be easily used as a reference. The data for each material is presented, including; the maximum static and dynamic loads, sliding velocity, PV value, temperature range, friction coefficient, wear, coefficient of linear expansion, thermal conductivity, surface roughness and surface hardness. Not all the properties and data were found for all the materials, but most of them are included. From these data, plots were conducted and all the materials were included to easily select the material needed for a specific application depending on the required conditions. Appendix 1 shows some of the plots and graphs constructed.

4.3 **Aluminium Bronze, Beryllium Copper and ToughMet Bearing Materials**

As mentioned before, beside the self-lubricating bearings, there are lubricated bearing materials that are of high importance. These materials combine properties that other materials wouldn't have together, such as; high strength, lubricity, wear resistance, high corrosion resistance, temperature resistance and others. Here three important materials are compared and all three materials are copper based. Aluminium Bronze is the material most widely used in the bushes for pin joints in the landing gear because of its has high strength, it is wear resistant and has relatively high coefficient of friction. Beryllium Copper is well known for its high hardness and strength which permits for very high loading without plastic deformation. It also has low wear rates and it decreases with increasing stress, which is exceptional and allows for bearing designs without worrying about the wear of the material. As for the ToughMet material, it is a relatively new material and a copper-nickel-tin spinodal alloy which was first made by Brush Wellman Company. It is a high strength alloy with a low friction coefficient which makes it very suitable for bushing and bearing.

1.1.5. **Aluminium Bronze**

Aluminum Bronze alloy consists of 85%Cu, 4%Fe and 11%Al and they have higher strength than other bronzes and are used in applications were with high impact or reversing load. In

comparison with other copper alloys, its high strength is coupled with exceptional corrosion resistance under varies operation conditions and it can also stand temperatures up to 400°C (Glaeser 1983). To get maximum corrosion resistance, the composition and manufacturing of the material is controlled. They show no deterioration in mechanical characteristics and performance under most atmospheric conditions, that is why it is the best known to be used in aircrafts. They also have very low oxidation rates at high temperatures and excellent resistance to sulphuric acid, sulphur dioxide and other combustion products.

However, because aluminium bronze has poor compatibility, embeddability, and conformability, it is best suited for heavy-duty, low-speed applications with plentiful lubrication. Aluminium bronzes require harder shafts than softer bearing materials. Proper alignment is more critical because of low conformability.

1.1.6. **Beryllium Copper**

The strength of the age-hardened beryllium copper is very close to steel, however it has excellent thermal conductivity. This material has been used for loads up to 345 MPa in aircraft applications, mainly the landing gear and the control system of the tail assembly (Glaeser 1983). It is able to function at very high temperatures up to 600°F, has tensile strength higher than 165 ksi and demonstrates excellent corrosion resistance. It has a good combination of reduced weight, wear resistance and anti-galling properties to prevent cold welding which us why it is well known to be used in landing gears. They are also used in many electrical conducting applications.

Beryllium copper has a thermal expansion that is nearly similar to that of steels, even stainless grades, where it was found that the alloy content does not affect the thermal expansion coefficient over the temperature range these alloys are used in. In the same assembly, steel and beryllium copper are compatible, due to having a close thermal expansion. Moreover, beryllium copper high strength alloys have lesser densities than normal specialty coppers, so the input material often gives more pieces per pound. Also an advantage of beryllium copper is that its elastic modulus is higher than other specialty copper alloys by 10%-20%. For that, as well as its strength and resilience properties, the chosen alloy is beryllium copper.However, it does not tolerate dirty lubricants and misalignments.

1.1.7. **ToughMet**

As mentioned before, ToughMet is a copper-nickel-tin alloy that is relatively new. It is a high strength alloy capable of yield strength up to 100 ksi and it is made of wrought or continuous

cast (Kusner et al. 2003). It can be made of sizes up to 0.635 meters and it provides good design flexibility and excellent machinabilty. It is cost and weight effective. It has a unique combination of strength, lubricity, and corrosion, high temperature and wear resistance under severe loading. Also, its low friction coefficient, corrosion resistance and non-magnetic characteristics provide advanced performance and reliability. It has excellent tribological properties as well.

ToughMet obliges a specific high degree of consistency of composition and microstructure at the foundation. A casting technology for this alloy structure has solved the problems of conventional static or continuous casting techniques by facilitating sizes up to 0.635 meters in diameter in single lot masses as large as 15 tons (Kusner et al. 2003). This patent technology EquaCast, allows consistency of composition and microstructure for an alloy structure with a large range of temperature.This closed head casting technology has a patented top ceiling with directed slots interjected between the top of the mold and the liquid in the outsized holding furnace. Molten metal at high speed planar jets are created by the cyclic removal of the billet which infiltrates the solidification zone and ruptures dendrites, constructs initials for refinement and leads to a very uniform solidification process and microstructure.

1.1.8. **Comparison Between Aluminium Bronze, Beryllium Copper and ToughMet**

There are no wear models that are capable of predicting the performance of copper-based bearing materials. Their known characteristics indicates how well their performance can be expected as bearings. Any data collected is obtained from extensive experimental testing.

4.3.1.1 **Performance Criteria**

Table 1: Comparison of Performance Criteria

	Aluminium Bronze	Beryllium Copper	ToughMet
Max Pressure (MPa)	200	700	690
Max PV (MPa.m/s)	4.38	18.5	9.63
Max Sliding Velocity (m/s)	6.1	4.9	2.03
Temperature Range (C)	-270 - 400	0 - 200	100 - 240
Coefficient of Friction	0.25 - 0.40	0.30 - 0.33	0.15 - 0.27

4.3.1.2 **Physical Properties**

Table 2: Comparison of Physical Properties

	Aluminium Bronze	Beryllium Copper	ToughMet
Thermal Conductivity (W/m.K)	60	107	40
Coefficient of Thermal Expansion (10-6 per °C)	16	17	16
Corrosion Resistance	Excellent	Excellent	High
Wear Resistance	Very High	Very High	High
Machinability	Good	Good	Excellent

Dave Krus, product marketing director for Materion's Engineered Products Group said, "The same engineers who figured this out for beryllium copper were the ones who figured it out for ToughMet. We've got a whole lot of brain power and engineering experience here. Without it, we wouldn't have a flat ToughMet product," They had the same objectives and goals in mind and engineered two very reliable bearing materials. However, the beryllium copper material is exceptional in its thermal conductivity and very high PV value, Aluminium bronze in its corrosion resistance and ToughMet in its low friction coefficient.

5 TEST RIG

Considering that a P-V diagram is the main method of characterisation for a journal bearing a test rig design was proposed that would be able to examine bearings and produce experimental results.

5.1 Tribological Analysis

Essential requirements were set for the test rig development. The main criteria of the test rig are the ability to examine multiple bearings under a combination of testing conditions, be able to produce quick results and offer readings for tribological properties such as the coefficient of friction. The operational conditions of primal concern are the sliding velocity and the pressure applied to the bearing. Thus a method was proposed where the test rig can securely apply a pressure and a surface sliding velocity on the bearing without interrupting its normal function.

The proposed solution is defined diagrammatically bellow:

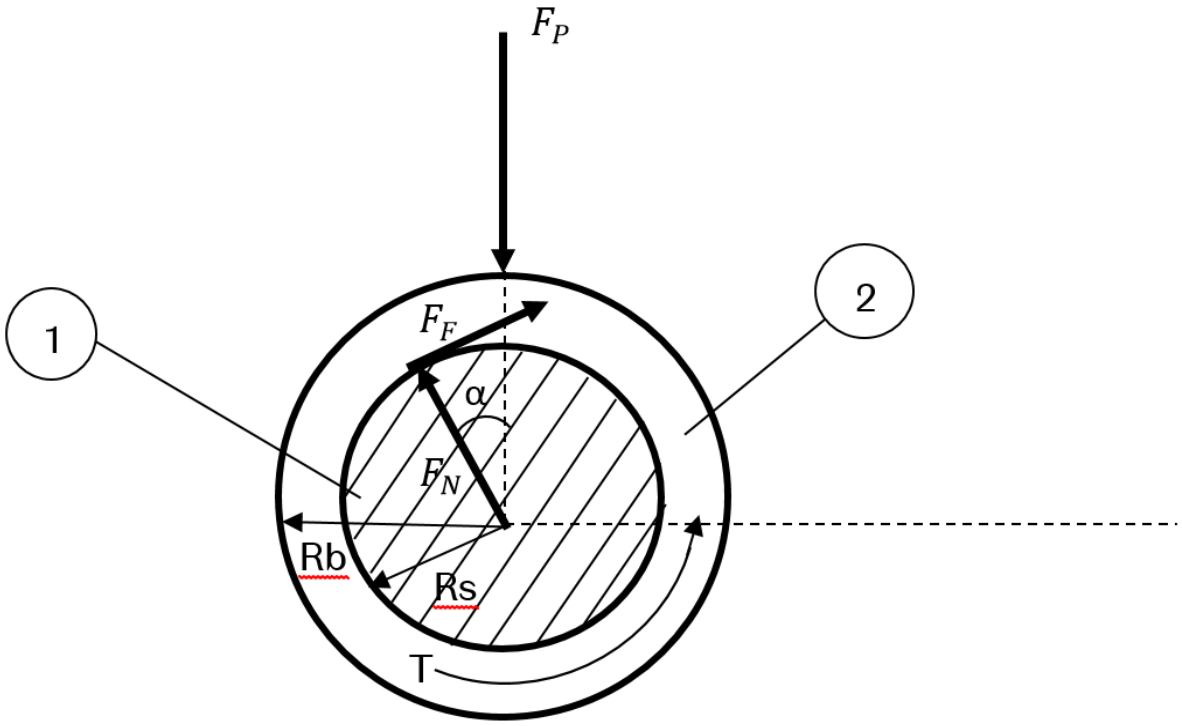

Figure 5.1.1 General view of the bearing being subjected to a normal load and a rotational speed.

The journal bearing slides over a central shaft (1). A normal load F_P is applied to the bearing that can be converted to a transferable pressure P according to the bearing dimensions.

Additionally the central shaft (1) will rotate with a torque T resulting in a sliding velocity V applied on the inner surface of the bearing.

The determination of the friction coefficient can be done by measuring the frictional torque T of the central shaft when the test rig will operate. Using the Coulomb's law the COF of interest is defined as the ratio of the tangential and normal reaction force component:

$$\mu = \frac{F_F}{F_N}$$

Equation 5.1.1

The test rig must be able to control the normal force F_P and the sliding velocity. Also important criteria is to transmit the normal load without causing any interruptions in the movement of the components allowing small rotations of the bearing. In addition in Figure 5.1.1 the two parameters Rs and Rb are the radii of the shaft and the bearing respectively. The reaction forces F_F and F_P are very difficult to be directly monitored, as a result they have to be calculated from the known torque T and the applied force F_P.Taking into consideration the force balance and the torque balance around the centre line of the bearing the reaction forces and the displacement angle α can be calculated:

$$\begin{cases} F_F = \frac{T}{Rs} \\ F_N = \sqrt{(F_P)^2 - \left(\frac{T}{Rs}\right)^2} \\ \sin(a) = \frac{\left(\frac{T}{Rs}\right)}{F_P} \end{cases}$$

Equation 5.1.2

Substituting the obtained equations into Equation 5.1.1 the coefficient of friction becomes:

$$\mu = \frac{1}{\sqrt{\frac{(F_P)^2}{(\frac{T}{Rs})^2} - 1}} = tan(a)$$

Equation 5.1.3

5.2 **Design Specifications**

The following requirements were set for test rig specifications:

- Capable of performing tests on multiple bushes simultaneously.
- Able to test both continuous and oscillatory motion.
- Capable to apply a maximum constant pressure of 100MPa on the bearing.
- Capable to run with a maximum sliding velocity of 2.5m/s on the surface of the bearing.
- Able to accommodate a journal bearing with inner diameter of 25mm.
- The rotational speed of the shaft and the applied pressure must be controllable.
- A convenient way to continually monitor the torque of the shaft.

The cost of build was carefully taken into account so that the manufacture of the test rig would be achievable in the future.

5.3 **Drawings**

1.1.9. **Initial Design**

The first version of the proposed solution is presented in Figure 5.3.1. In this version the test rig is capable to test two bearings simultaneously. A basic rectangular frame was produced that accommodates an electric motor (3) responsible to transmit the motion to the two shafts. To ensure the uniformity of the test rig the motor was placed in the middle of the structure with both shafts in each side. In this specific design the bearing samples can be tested only in an oscillatory motion via the crank-shaft system (4). The rotary motion of the motor is convert into a linear movement like piston via the big lever. A small arm linked to that lever is attached to the shaft, causing the shaft to rotate forwards and backwards (oscillatory motion).Two bearing units (2) support the shaft. The bushing slide over the shaft and is securely located in a bearing house (2). Dead-weights hanged on an arm that extends vertically from the bearing house are responsible to apply the radial load (2).

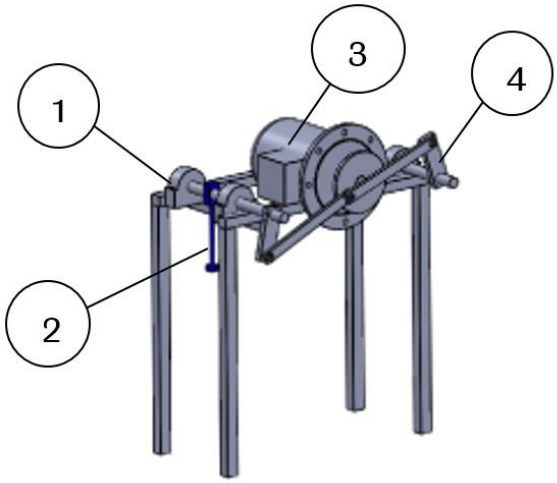

Figure 5.3.1: Isometric view of the initial design of the proposed test rig

1.1.10. **Design 2**

An upgraded version of the initial design is presented in this section where several problems from the previous test rig that have been solved. The limitation to test the bearings under oscillatory motion only was the first problem to be tackled. A coupling rod (1) has been introduced to the design to transmit the rotational motion of the motor (2) to the two side shafts. The frame of the test rig has been upgraded to improve its rigidness. Considering the design specifications that were set, the maximum pressure of 100MPa would not be feasibly achievable using the dead-weights system. Two hydraulic power packs (3) were employed which will permit the application of the required pressure to the journal bearings. A research has been conducted for the bearing units required to support the two shafts under the maximum testing conditions. Two new bearing houses have been designed which can accommodate roller bearings, capable to support the two shafts.

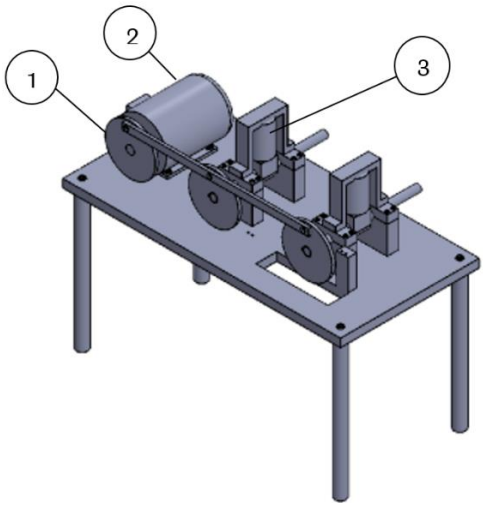

Figure 5.3.2: The second design in isometric view.

1.1.11. **Final Design**

The final version of the test rig is presented in Figure 5.3.3. Utmost efforts have been made to construct a test rig design capable to fulfil the design specifications stated above. All the technical problems determined in the previous designs have been tackled in this test rig. An exploded view of the test rig is presented in Figure 5.3.4, that aids in the understanding of the test rig's functionality. A significant improvement in the design is the ability to perform both a continuous and oscillatory motion testing. This is achievable by replacing the red parts (1) with the green parts (6) to switch from continuous to oscillatory movement. The two mechanisms have been designed with the prospect to be engaged and disengaged from the test rig easily. The essential requirement of the design to measure the frictional torque of the two shafts has been satisfied with the introduction of two torque transducers (2). Additionally the electric motor (5) has been changed with a more suitable one, capable to drive the shafts with the required speed of 2.5m/s. Due to its considerable weight the motor is mounted on the ground. An additional shaft has been introduced which is located at the same level with the other shafts. A timing belt (4) transmits the motion from the motor to the central shaft which is then distributed to the two side shafts. Pillow blocks have been replaced the bearings units used in previous designs.

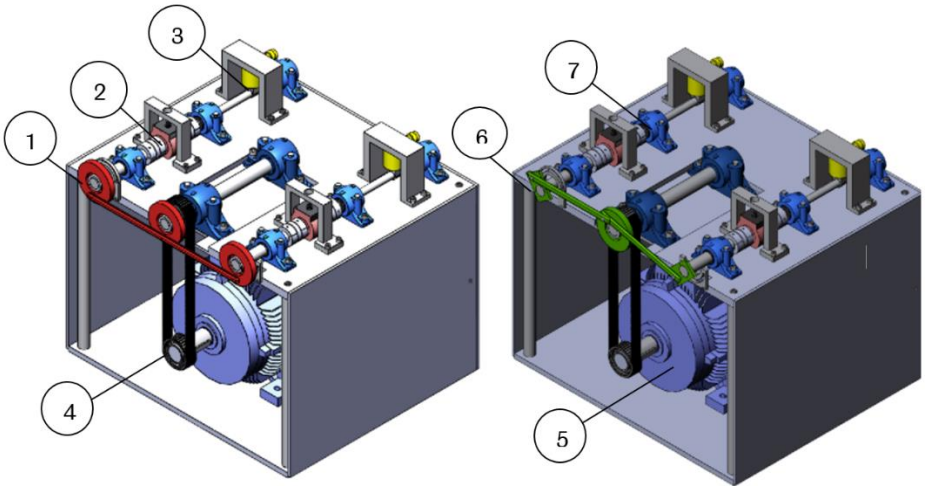

Figure 5.3.3: The proposed test rig design presented in two forms, continuous and oscillatory motion.

Part List		
Item No	Component	Qty
1	Hydraulic Cylinder	2
2	Legs	4
3	Torque sensor housing	2
4	Pillow blocks	8
5	Torque sensor coupling	4
6	Torque sensor	2
7	40mm shaft	2
8	Top Crank Guide	1
9	Crank Arm	2
10	Crank System	1
11	Main Disk	1
12	Timing belt	1
13	Motor	1
14	25mm shaft	2
15	Bush	2
16	Bush housing	2
17	Top plate	1

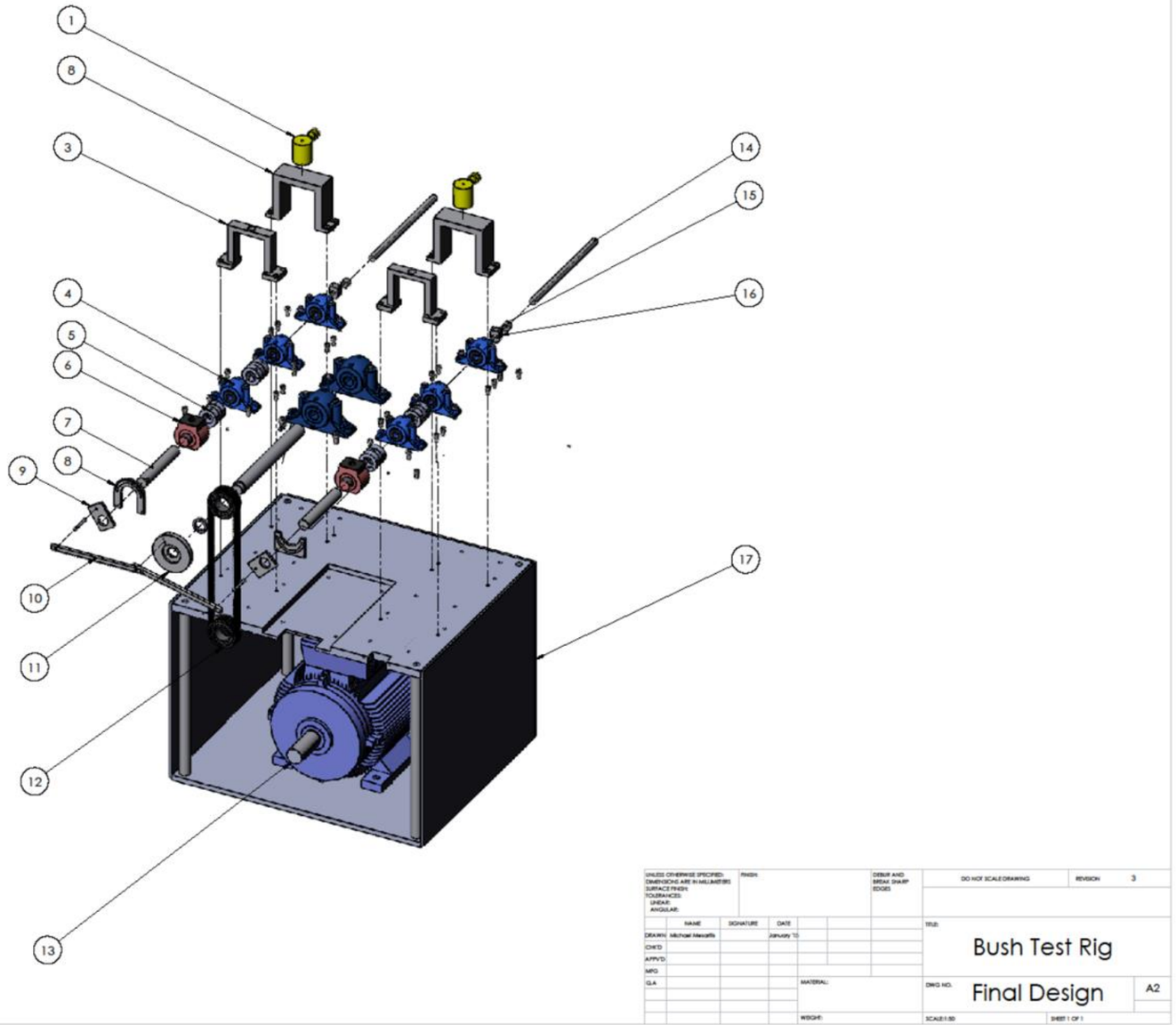

Figure 5.3.4: Exploded view of final design

5.4 **Instrumentations**

1.1.12. **Sizing Motor**

Considering the maximum operational conditions of 100MPa pressure and 2,5m/s sliding velocity, the required torque was calculated. Collecting data from many bearings a 0.4 coefficient of friction was assumed in a 'worst case' scenario. Moreover using the bearing dimensions, the power required was calculated using the following equations:

$$\begin{cases} F_P = P \times d \times w \\ T = \mu \times F_P \times Rs \\ P = T \times \omega \end{cases}$$

Equation 5.4.1

Using the Equation 5.4.1 and by inputting the relevant factors a power of 17kW was calculated. The motor selected is a 3-phase AC motor capable to deliver 37,5kW allowing a factor of safety over 2. An inverter drive is coupled with the motor allowing the output speed to be adjusted. Full working can be found in Appendix 2-Sizing Motor.

1.1.13. **Hydraulic Power Cylinder**

As mentioned in previous sections the proposed method to create a force up to the desired testing values involves the use of a hydraulic power cylinder. Utilising equations 2. 4 the force required for a testing under maximum conditions is a 25kN radial load. An Enerpac hydraulic cylinder with model number RCH 101 would be capable to provide up to 100kN thrust force. Further details in Appendix 3-Hydraulic Power Pack.

1.1.14. **Torque Sensor**

A criteria equally important to determine the experimental coefficient of friction is to continuously monitor the torque of the shaft. A torque of 125Nm was calculated based in maximum operational conditions and utilising equations 2.4. The method selected to observer the torque was by attaching a torque transducer to the shaft. A FUTEK rotary torque transducer was selected with model number TRS300. The transducer is also capable to provide readings for the rotating speed, allowing a validation of the inverter's accuracy. Further specification details in Appendix 4-Torque transducer.

6 WEAR PREDICTOR MODELLING

6.1 Introduction

Two predictive were models were required, one for each mode of operation the bearings may face. Firstly, a model to predict the wear of a rotating contact was developed. Secondly, a model has been developed to determine the wear experienced when a bearing undergoes cyclic tensile and compressive loading.

6.2 Methodology

1.1.15. Archard's Wear Equation

Archard's wear equation as shown in Equation 4.1.1 will be used to calculate all wear volume losses, it is used due to its simplicity and small number of input variables. Firstly, the sliding distance must be calculated, to do this it is necessary that the true nature of the contact between the bearing and the pin is known.

1.1.16. Hertzian Analysis

The sliding distance is greatly dependent upon the contact area, Hertz theory is used as a first approximation of the contact area. Dependent upon how conformal the contact of the two bodies is, the contact between a pin and a bearing can be approximated as being rectangle in area with an elliptical pressure distribution, this is show below in Figure 6.2.1.

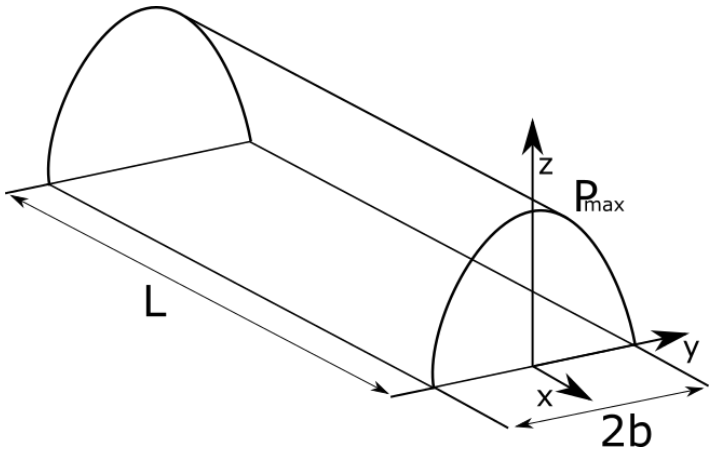

Figure 6.2.1: Schematic showing a rectangular contact area with elliptical pressure distribution, adapted from (Priest 2014).

Figure 6.2.1 shows a rectangle contact area that would be produced when the pin and bearing come into contact. The variable L represents the length of the pin/bearing, 2b represents the contact width, and P_{max} indicates that the maximum pressure in the contact is located along the centreline. The half width of contact area can be calculated by using Equation 6.2.1 below.

$$\mathrm{b} = \left(\frac{8\mathrm{WR}}{\pi \mathrm{LE}'}\right)^{\frac{1}{2}}$$

Equation 6.2.1

It can be seen that in order to calculate the half width of contact, we first need to calculate E' and R. E' is known as the Equivalent Modulus and R represents the Curvature sum, thisis used in order to re-frame the problem as a cylinder of radius R, acting upon on a flat plane.

$$\mathrm{R} = \left(\frac{1}{R_1} + \frac{1}{R_2}\right)^{-1}$$

Equation 6.2.2

Where:

R_1 = Radius of pin, m R_2 = Radius of bearing, m

R_1 and R_2 can be either positive or negative; representing convex and concave surfaces, respectively. Therefore, in this work R_1 is positive and R_2 is negative. E' is used as another equivalency is used in Hertz theory in order to re-frame the problem as a perfectly elastic cylinder acting upon a perfectly rigid plane as the counterface (Priest 2014). The equation for this, calculating the equivalent modulus is shown below.

$$E' = \frac{2E_1E_2}{(1-{\upsilon_1}^2)E_2 + (1-{\upsilon_2}^2)E_1}$$

Equation 6.2.3

Inputting Equation 6.2.2 and Equation 6.2.3 in Equation 6.2.1 yields the half contact width b. This value can further be used to in Equation 6.2.4, below, allowing us to find a suitable value to sliding distance to be used in Equation 4.1.1..

$$D = 2bC$$

Equation 6.2.4

It is shown in Figure 6.2.1 that the location of the maximum pressure is located along the centreline. It is possible, given the information already available to calculate values for maximum pressure and mean pressure. Equations for P_{max} and P_{mean} can be seen below in Equation 6.2.5 and Equation 6.2.6.

$$P_{max} = \left(\frac{WE'}{2\pi RL}\right)^{\frac{1}{2}}$$

Equation 6.2.5

$$P_{mean} = \left(\frac{\pi WE'}{32RL}\right)^{\frac{1}{2}}$$

Equation 6.2.6

6.3 **Oscillatory and continually rotating contact**

The first mode of wear to be investigated is volume wear loss occurring when a loaded bearing rotates around a pin, this can be continuous rotation or oscillatory. Figure 6.3.1, below illustrates continuous rotational movement.

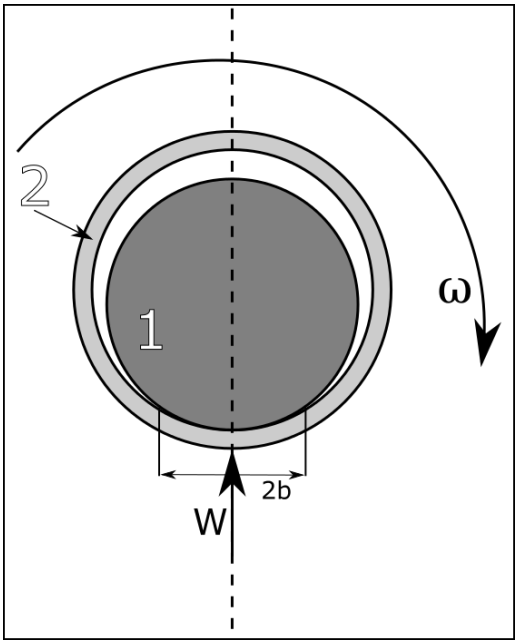

Figure 6.3.1: Schematic of rotational contact

It can be seen in Figure 6.4.1that the force is applied to bottom of the bearing, causing contact with the pin.

6.4 **Contact due to tension and compression**

The second mode of wear to be investigated is the wear loss that occurs when a pin and bearing pair undergo cyclical tensile and compressive loading. A schematic of the overall arrangement is shown below in 6.4.2.

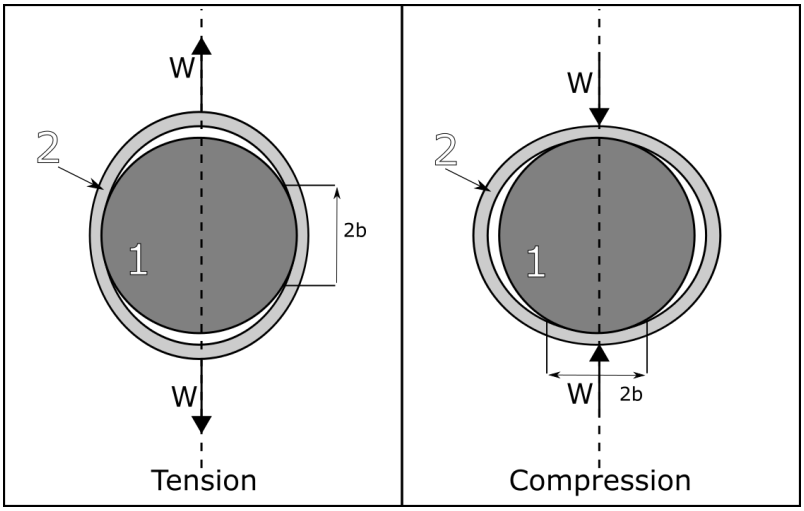

Figure 6.4.1: Schematic of tension and compression contact

It is shown in Figure 6.4.1 that the force is applied at both the top and the bottom of the bearing. The effect of both tensile and compressive loading is shown, it is evident that for each cycle of compression then tension there will be four contact areas. This work will model just one contact area and multiply the resultant wear by four to approximate the complete wear on the whole bearing.

The pin is made of a much harder material than the bearing, and as such when the two materials come into contact there is elastic deformation of the bearing (Yampolski et al. 1981). It is believed that this elastic deformation or microslip of the softer material against a harder surface leads to wear (Olofsson 1995; Antoni et al. 2007). An illustration of the microslip process is shown below in 6.4.2.

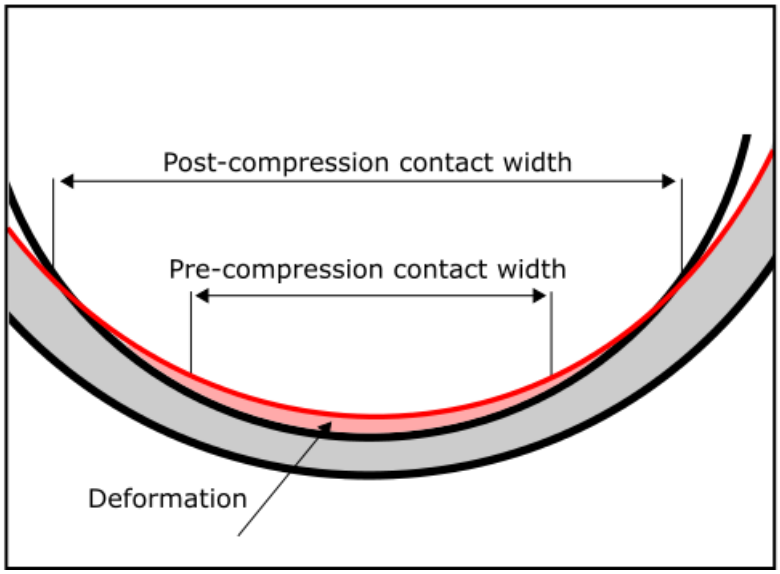

6.4.2: Demonstration of microslip due to impact and the resulting deformation

6.4.2 shows that as the load is increased on the bearing there is greater contact with the pin. The extent to which the material deforms is analogous to the sliding distance that is shown in Equation 4.1.1. Johnson (1987) describes an equation for determining the stress in the surface due to non-Hertzian normal contact of elastic bodies, this is shown by Equation 6.4.1, below.

$$\sigma = 1.185(1 - 0.23\nu)\mu P$$

Equation 6.4.1

With the surface stresses known, it is possible to use the fundamental definition of Young's modulus to generate a corresponding strain, the equation for which is shown below.

$$E_2 = \frac{\delta}{\varepsilon} \therefore \varepsilon = \frac{\delta}{E_2}$$

Equation 6.4.2

Strain is a non-dimensional value and as such represents a percentage extension; this can be used to generate a sliding distance, D to be used in Equation 4.1.1.

1.1.17. **Initial micro-slip model**

Prior to the work shown above, a different approach was considered based upon the work by Hagman & Olofsson (1998), this work focused on the premise of asperities deforming against a flat plate with the asperities being treated as ellipsoidal bodies. Hagman and Olofsson's work did not capture the information required for this project and a different

approach was decided upon. The full workings of this initial approach can be seen in Appendix 5.

6.5 **Discretisation of contact area**

Using the values calculated with the above equations it is possible to approximate the wear volume in this system. However, to generate a more accurate value for wear loss, the contact area was discretised with n number of nodes and is illustrated below.

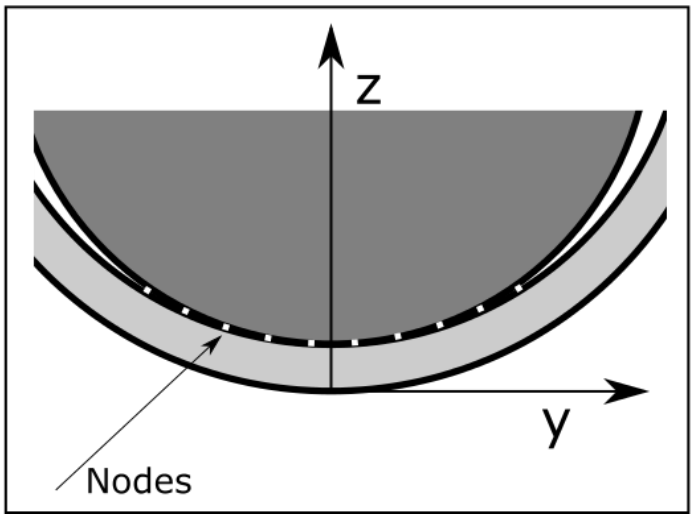

Figure 6.5.1: Schematic showing pin, bearing and the location of nodes

The use of nodes enables a full pressure distribution to be calculated, allowing for a more accurate wear volume, an equation for pressures at each node is shown below (Johnson 1987).

$$P_i = P_{max}\left(1 - \left(\frac{y}{b}\right)^2\right)^{\frac{1}{2}}$$

Equation 6.5.1

6.6 **Results**

The models created in this work are used to predict the resultant wear when a PTFE bearing interacts with a steel bearing. PTFE was chosen as a bearing material due to the wide availability of its material and mechanical properties. Each model used the same values for pin/bearing diameters, Young's modulus, Poisson's ratio, contact length, number of nodes, load and number of cycles.

1.1.18. **Oscillatory and continually rotating contact**

User Inputs	
Pin Diameter (m)	0.025
Pin Elastic Modulus (E1)	2.00E+11
Pin Poissons Ratio (v1)	0.3
Bush Diameter (m)	-0.03
Bush Elastic Modulus (E2)	5.00E+08
Bush Poissons Ratio (v2)	0.46
Bush Length	0.025
Motor Speed (RPM)	1000
Time (Mins)	1
Oscillation angle	360
Number of Cycles	1000
Number of Nodes	25
Normal Load	625
Wear Coefficient	1.00E-05

Calculation Values	
Curvature Sum (R)	0.075
Equivalent elastic modulus (E')	1264742151
Half Length (b)	0.001942986
Arc Length Each Panel	0.000161916
Number of Positions	13
Sliding Distance	3.885972228
Pmax (MPa)	8.191254788
Pmean (MPa)	6.433396467

Output Values	
Wear Loss (loading profile)	0.024069178
Wear Loss (single Point)	0.024287326

Loading Profile		Wear Volume Loss
Position Number	Force at each node	
13	0.000	0
12	13.251	0.000514945
11	18.328	0.000712236
10	21.931	0.000852251
9	24.714	0.000960378
8	26.931	0.001046548
7	28.715	0.001115859
6	30.142	0.001171307
5	31.261	0.001214793
4	32.104	0.001247568
3	32.694	0.001270461
2	33.042	0.001284001
1	33.157	0.001288483
2	33.042	0.001284001
3	32.694	0.001270461
4	32.104	0.001247568
5	31.261	0.001214793
6	30.142	0.001171307
7	28.715	0.001115859
8	26.931	0.001046548
9	24.714	0.000960378
10	21.931	0.000852251
11	18.328	0.000712236
12	13.251	0.000514945
13	0.000	0

Figure 6.6.1: Tables showing user input, calculation and output values for rotating wear model. Wear volume at each node is also shown.

Figure 6.6.1 shows the resultant wear that would be experienced by a PTFE bearing when paired with a steel pin under continuous rotation. A wear volume loss of approximately 0.024 m^3 is predicted by the model for 1000 cycles with a normal force of 625N.

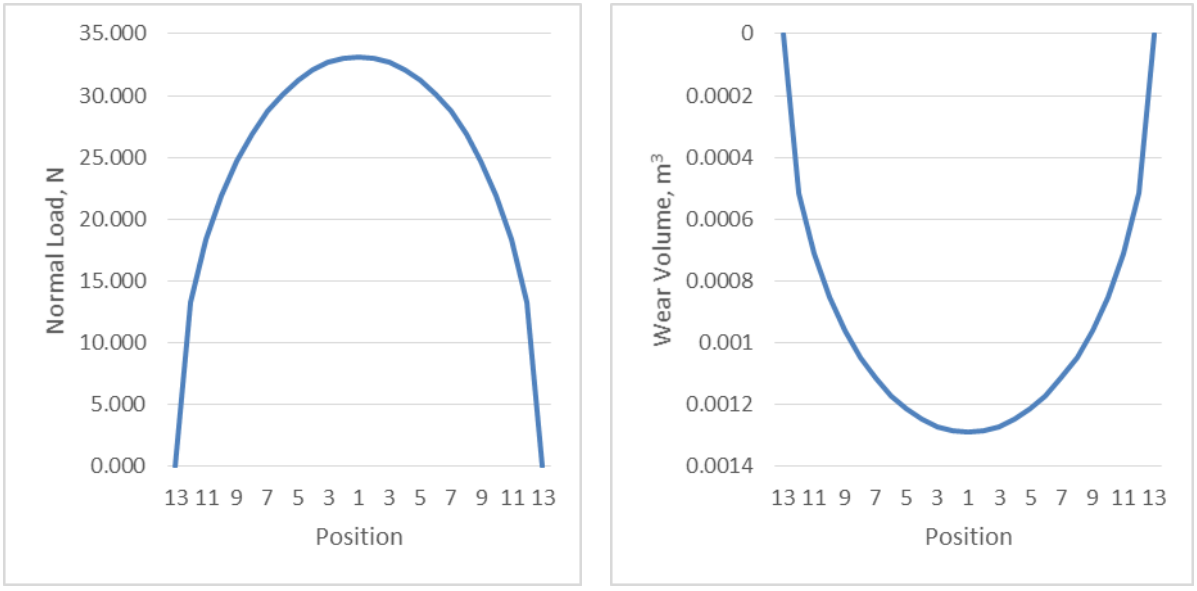

Figure 6.6.2: Profiles showing how load and wear volume change with nodal position

Figure 6.6.2 shows the elliptical distribution that occurs when the bearing is loaded, alongside this there is also a plot of wear volume at each nodal position. The curve of the wear volume graph is representative of the wear track produced from this wear.

1.1.19. **Contact due to tension and compression**

User Inputs	
Pin Diameter (m)	0.025
Pin Elastic Modulus (E1)	2.00E+11
Pin Poissons Ratio (v1)	0.3
Bush Diameter (m)	-0.03
Bush Elastic Modulus (E2)	5.00E+08
Bush Poissons Ratio (v2)	0.46
Bush Length	0.025
Coefficient of Friction	0.05
Number of Cycles	1000
Number of Nodes	25
Normal Load	625
Wear Coefficient	1.00E-05

Calculation Values	
Curvature Sum (R)	0.075
Equivalent elastic modulus (E')	1264742151
Half Length (b)	0.001942986
Arc Length Each Panel	0.000161916
Number of Positions	13
Sliding Distance	0.004151476
Pmax (MPa)	8.191254788
Pmean (MPa)	6.433396467

Nominal Loading (1N)	
Half Length (b)	7.77194E-05
Arc Length Each Panel	6.47662E-06

Output Values	
Wear Loss (loading profile)	0.029418984
Wear Loss (single Point)	0.027023082

Loading Profile					Wear Volume Loss
Position Number	Pressure at each node	Stress	Strain	Sliding Distance	
13	0.000	0.000	0	0	0.00E+00
12	3273656.494	173442.740	0.000346885	8.98658E-06	2.94E-04
11	4527886.449	239893.537	0.000479787	1.24296E-05	5.63E-04
10	5418005.774	287053.260	0.000574107	1.48731E-05	8.06E-04
9	6105400.843	323472.379	0.000646945	1.67601E-05	1.02E-03
8	6653206.321	352495.853	0.000704992	1.82639E-05	1.22E-03
7	7093834.736	375840.941	0.000751682	1.94734E-05	1.38E-03
6	7446336.695	394516.971	0.000789034	2.04411E-05	1.52E-03
5	7722789.076	409163.791	0.000818328	2.12E-05	1.64E-03
4	7931148.345	420202.946	0.000840406	2.1772E-05	1.73E-03
3	8076686.142	427913.735	0.000855827	2.21715E-05	1.79E-03
2	8162763.381	432474.224	0.000864948	2.24078E-05	1.83E-03
1	8191254.788	433983.737	0.000867967	2.2486E-05	1.84E-03
2	8162763.381	432474.224	0.000864948	2.24078E-05	1.83E-03
3	8076686.142	427913.735	0.000855827	2.21715E-05	1.79E-03
4	7931148.345	420202.946	0.000840406	2.1772E-05	1.73E-03
5	7722789.076	409163.791	0.000818328	2.12E-05	1.64E-03
6	7446336.695	394516.971	0.000789034	2.04411E-05	1.52E-03
7	7093834.736	375840.941	0.000751682	1.94734E-05	1.38E-03
8	6653206.321	352495.853	0.000704992	1.82639E-05	1.22E-03
9	6105400.843	323472.379	0.000646945	1.67601E-05	1.02E-03
10	5418005.774	287053.260	0.000574107	1.48731E-05	8.06E-04
11	4527886.449	239893.537	0.000479787	1.24296E-05	5.63E-04
12	3273656.494	173442.740	0.000346885	8.98658E-06	2.94E-04
13	0.000	0.000	0	0	0.00E+00

Figure 6.6.3: Tables showing user input, calculation and output values for compression wear model. Wear volume at each node is also shown.

Figure 6.6.3 shows the necessary data required to approximate this form of wear. Values for a half-length and arc length can be seen for a nominal loading of 1N, these lengths are used in conjunction with the strain values to estimate a sliding distance. A nominal loading of 1N represents the pin and bearing just touching with limited deformation. The resultant wear

volume loss has been approximated as $0.029m^3$, this is a combined value for all four contacts throughout each cycle.

6.7 **Analysis**

It can be seen that Figure 6.6.1 and Figure 6.6.3 show two results for the output values, the two values represent the approximate wear when the load is treated as acting on a single point and when the surface has been discretised.

Figure 6.6.1 and Figure 6.6.3 show that the total wear volume loss for both modes of wear is very similar for the same material properties and number of cycles, $0.024m^3$ and $0.029m^3$ respectively. Intuitively, you would think that the wear due formed under cyclical tensile and compressive loading would be much smaller than that caused by frictional contact. Similarity between the wear modes is most likely attributed to the fact that the second mode has four times the number of contacts.

Whilst this work has produced two seemingly accurate models for approximating the wear on a bearing there is a problem the proposed models. Hertzian analysis is limited to perfectly elastic solids with frictionless surfaces (Priest 2014). Further to this, Hertz theory is only recommended for surfaces with low conformity and is therefore a good first approximation for determining the contact area. However, the theory breaks down as the difference in radii of the bearing and pin decreases, resulting in higher conformity. Johnson (1987) proposes a counter approach specifically for highly conformal contacts. With more time this approach would be implemented into the models to provide a higher accuracy of wear prediction.

Furthermore, neither of the models has been validated by experimental methods due to time constraints. With more time I would perform tests with the same set ups as shown in Figure 6.3.1 and Figure 6.4.1.. The testing rig shown in Section 5 would fit the needs perfectly for reproducing the tests shown in Figure 6.3.1.

7 CONTAMINANT SAMPLE TESTING

7.1 Introduction

In order to see how the wear and friction properties of typical materials found in aircraft were affected by contamination, three materials were contaminated with two separate chemicals. The two contaminants were:

- Skydrol, a hydraulic fluid commonly found in aircraft landing gear
- De-icer

The Three different materials were:

- Trelleborg Orkot 410
- RBC HP Liner
- Saint-Gobain Meldin 5330

A Bruker Universal Mechanical Tester (UMT) as shown in Figure 1 was used to create wear tracks in the materials. A script was used which inputted the required parameters; number of cycles, distance and load. The load is varied between the materials to keep the contact pressure constant which allows comparison between the results as the contact conditions are the same.

The wear tracks were measured using a profilometer as shown in Figure 2 at three points along the track to get an average for the depth and width of the profile. This profile data is used to calculate the wear volume and hence the wear coefficient using Archards wear equation show in Equation 4.1.1.

The wear coefficient characterises the wear of the material due to the contact conditions and so can be more useful property to use as a comparison between the materials then wear volume by itself.

Figure 7.1.2: Bruker UMT

Figure 7.1.2: Profilometer

7.2 **Results**

Figure 3 shows the results of the experiments. It shows that there is not a significant change in the friction coefficient between the two contaminants for any of the three materials which suggests that contamination has little effect on the coefficient of friction of the material.

It shows that for the HP liner there is not a significant change in wear coefficient between the two contaminants but for meldin and orkot, the de-icer produces an increase in wear rate compared to the skydrol.

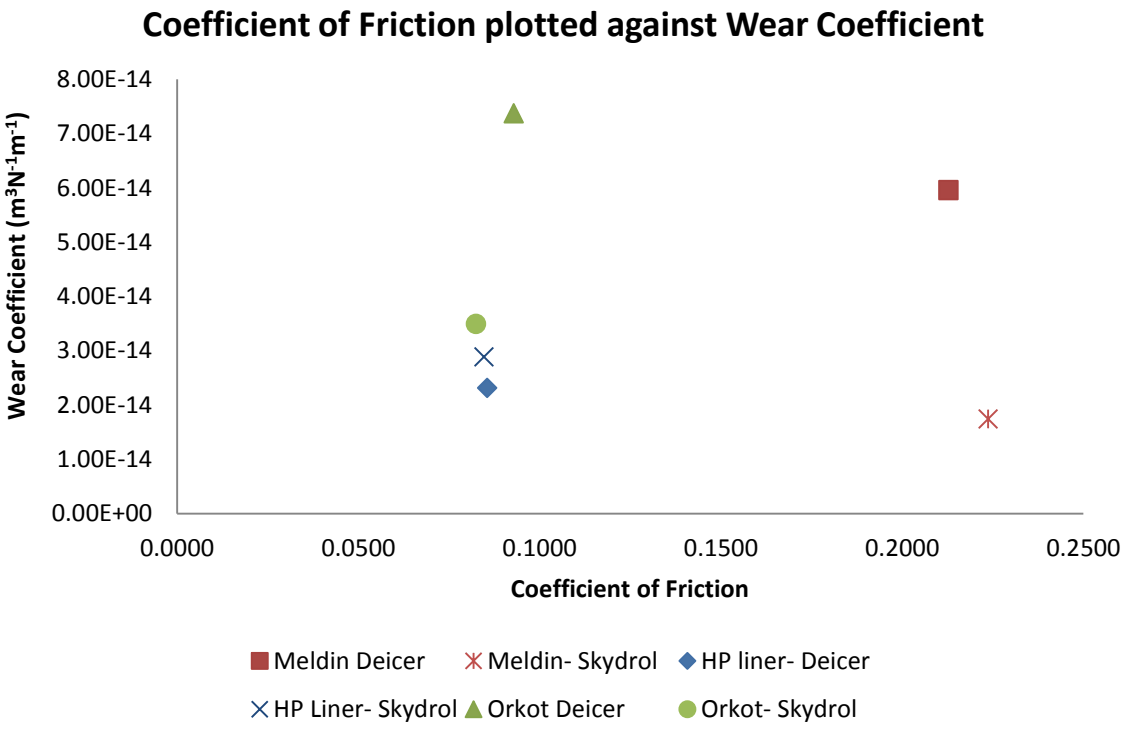

Figure 7.2.1: Chart displaying contaminant sample testing results

7.3 **Microscopic Analysis**

To investigate the wear tracks formed by the testing a microscope was used. In Figure 7.3.1 coupons' surfaces can be observed after the testing. In both rows starting from left to right the materials presented are HP Liner, Meldin 5330 and Orkot. In the top row the materials have been treated with De-Icer and in bottom by Skydrol. The results obtained comply with the post-processing comparison of the wear coefficient. In the HP-Liner case similar wear tracks can be observed in both cases indicating that the wear coefficient was similar in both cases. Regarding the Meldin 5330 there is a distinct difference in the wear tracks. The surface affected by De-Icer exhibits wider wear marks compared with the coupon affected by Skydrol. In terms of the Orkot coupons unusual wear was captured. There isn't uniform linear groove on the worn surface similarly to the other two materials. It appears that some lateral surface cracks can be detected caused by the shear stress. Moreover comparing the two Orkot coupons the De-Icer affected surface shows more damage than the other.

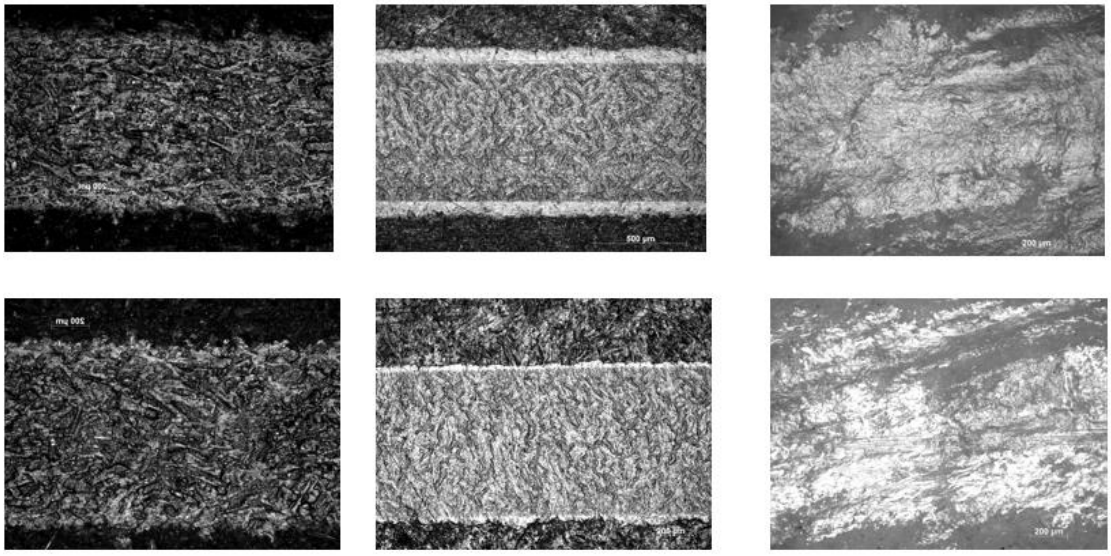

Figure 7.3.1: Images from the microscopic investigation.

7.4 **Analysis**

The wear coefficient data cannot be accurately relied upon without further testing. This is because the calculation of the wear volume has a degree of error in it due the fact that the wear track is assumed to be the same cross section along the wear track with the width and depth of track averaged from three measurements. A more accurate way of measuring the volume lost is to equate the volume loss to mass loss during the test. However due to samples being relatively small and light the scales used would have to be extremely accurate to represent the volume loss correctly

For Orkot the thickness of the fibres is a similar degree to the depth of the wear track. This means the results for this material do not accurately represent the properties of this material; this could be easily counteracted by creating a deeper wear track to penetrate through the layers of fibres.

Additionally there was an issue with the second meldin skydrol test. A much larger wear track was created despite the parameters being identical to the other two runs and the reason for the problem remains unidentified. Due to the lack of space on the samples, this run was simple omitted from the analysis.

7.5 Further work

There are a number of things which could be explored to corroborate the findings from this experiment and improve the understanding of the effect of contamination

- Uncontaminated samples can be tested to check the effect of contamination compared to the clean material
- A more accurate procedure for calculating the wear coefficient should also be carried out. If a deeper wear track is created by increasing contact pressure, or just running the test for longer, than there would be a greater mass loss which should allow for the weighing method mentioned in section Analysis to be used.
- Analysis of the wear particles and further microscopy analysis would show if there is a change in the wear mechanism between the two different contaminants.

8 LANDING GEAR BUSH TESTING

Using a test rig available nicknamed 'Olive' two dry rubbing bearings would be tested to analyse their wear properties. The test would be carried out under normal working loads and speed experienced in an aircraft landing gear to identify their suitable to replace current lubricated bearings. The test parameters would first need to be worked out using data provided from airbus from their field trial of a landing gear rig.

To roundness of the bushes is measured before and after the test, along with the mass of the bush. The bushes are heated slightly to 50°C overnight to remove any moisture from them. Using a Talyrond measurement machine the roundness of the bush can be found, unfortunately the machine was not calibrated correctly which meant the roundness was not able to be found. This meant the test was unable to take place during the timescale of this project as the results would not useful without being able to compare the initial to final roundness profiles.

9 CONCLUSION

The landing gears structural weight accounts for about 57% of that of the aircraft. The numerous greasing pints incorporated in the aircraft to lubricate and protect bushes against contamination also proves time-consuming and costly, adding to the weight of the landing gear. Efforts have been made to potentially implement weight-saving features of the aircraft landing gear airbus A320 through the use of self-lubricating or dry-rubbing bearings. Self-lubricating materials have been surveyed on a wide scale, and their properties compared. A detailed and relevant comparison between Aluminium Bronze, Beryllium Copper and TougMet has also been made.

We are aware that characterization of the aircraft journal bearing material properties is successfully achieved through P-V (pressure velocity) diagrams. This led to a proposed test-rig design of high competency, allowing simultaneous and rapid testing of the bushes under high pressures and sliding velocities similar to those experienced in real-life applications.

Models predicting the wear and micro slip of a given material were proposed and generated. Archard's wear laws, and Hertzian contact analysis were used in the implementation of the models. The contact due to tension and compression was also calculated in order to relate wear to micro-slip phenomenon.

Contamination tests were conducted on three material samples frequently used in aircraft. These were; RBC HP Liner, Saint-Gobain Meldin 5330 and Trelleborg Orkot 410, tested against the chemicals skydrol and De-icer. Wear coefficients were found using Archard's wear law and plotted against the friction coefficient. A detailed microscopic analysis was also done to investigate the wear tracks witnessed.

Future work would include building the proposed testing rig in order to test the materials suggested due to the material survey. The test rig will also be used to validate the predictive wear models and to perform more in-depth and accurate contamination tests.

10 REFERENCES

Antoni, N. et al., 2007. On the cumulative microslip phenomenon. *European Journal of Mechanics - A/Solids*, 26(4), pp.626–646.

Archard, J.F., 1986. Friction between metal surfaces. *Wear*, 113(1), pp.3–16.

Archard, J.F., 1980. Wear theory and mechanisms. *Wear control handbook*, 58.

Brookes, K., 1980. Antifriction materials. , 5(89).

Christy, R.I., 1982. Dry Lubrication for Rolling Element Spacecraft Parts. *TRIBOLOGY international*.

Eliezer, Z. et al., 1978. High speed tribological properties of graphite fiber/Cu-Sn composites. , 49(1).

Evans, D.C. & Senior, G.S., 1982. Self-lubricating materials for plain bearings. *TRIBOLOGY international*.

Fusaro, R.L., 1990. Self-Lubricating Polymer Composites and Polymer Transfer Film Lubrication for Space Applications. *TRIBOLOGY international*.

Glaeser, W.A., 1983. Wear Properties of Heavy Loaded Copper-Based Bearing Alloys. *Journal of Metals*.

Hagman, L. a & Olofsson, U., 1998. A model for micro-slip between flat surfaces based on deformation of ellipsoidal elastic asperities—parametric study and experimental investigation. *Tribology International*, 31(8), pp.209–217.

Johnson, K.L., 1987. *Contact mechanics*, Cambridge university press.

Kozma, M., 2001. Load-Carrying Capacity of Lubricated and Dry Sliding Elements. *Lubrication Science*.

Kusner, R.E. et al., 2003. *Engineering Guide: ToughMet ® 3AT (C72900) ToughMet ® 3CX (C96900)*, Brush Wellman.

Lancaster, J.K., 1973. Dry bearings: a survey of materials and factors affecting their performance. *Tribology*, 6(6), pp.219–251.

Morgan, V.T., 1979. Bearing materials by powder metallurgy.

Olofsson, U., 1995. Cyclic micro-slip under unlubricated conditions. *Tribology International*, 28(4), pp.207–217.

Pratt, G.G., 1969. A review of sintered metal bearings: their production, properties, performance performance.

Priest, M., 2014. MECH5570M Introduction to Tribology.

Shvedkov, E.L., 1983. Self-lubricating Bearing Materials - A Survey. *Institute of Materials Science, Academy of Sciences of the Ukrainian SSR*.

Stachowiak, G.W. & Batchelor, A.W., 2014a. Chapter 11 - Abrasive, Erosive and Cavitation Wear. In G. W. Stachowiak & A. W. Batchelor, eds. *Engineering Tribology (Fourth Edition)*. Boston: Butterworth-Heinemann, pp. 525–576.

Stachowiak, G.W. & Batchelor, A.W., 2014b. Chapter 12 - Adhesion and Adhesive Wear. In G. W. Stachowiak & A. W. Batchelor, eds. *Engineering Tribology (Fourth Edition)*. Boston: Butterworth-Heinemann, pp. 577–596.

Williams, J.A., 2005. Wear and wear particles—some fundamentals. *Tribology International*, 38(10), pp.863–870.

Yampolski, G.Y., Kragelskii, I. V & Yushakov, I. V, 1981. Abrasive wear of rolling bearings. *Tribology International*, 14(3), pp.137–138.

Zhu, J., Pugh, S. & Dwyer-Joyce, R., 2012. Model and experiments to determine lubricant film formation and frictional torque in aircraft landing gear pin joints. *IMECHE*, 226(4).

11 APPENDICES

11.1 Appendix 1- Material Selection Excel Sheet Work

Company Name	Website
GGB	http://www.ggbearings.com/en
Saint-Gobain	http://www.bearings.saint-gobain.com/Default.aspx
CSB	http://www.csbslidingbearings.com/
Rexnord	http://www.rexnord.com/Pages/Home.aspx
KAMAN	http://www.kaman.com/home/
Polygon	http://polygoncomposites.com/
Bowman	http://www.bowman.co.uk/home
RBC	http://www.rbcbearings.com/index.asp
SBS	http://www.sbs-bearings.com.sg/home/
igus	http://www.igus.com/
SKF	http://www.skf.com/us/index.html
Vesconite	http://www.vesconite.co.za/
Trelleborg	http://www.orkot.com/en/home/homepage.html
Daemar	http://daemar.com/

Figure 11.1.1: List of Self-Lubricating Material Bearing Companies Surveyed

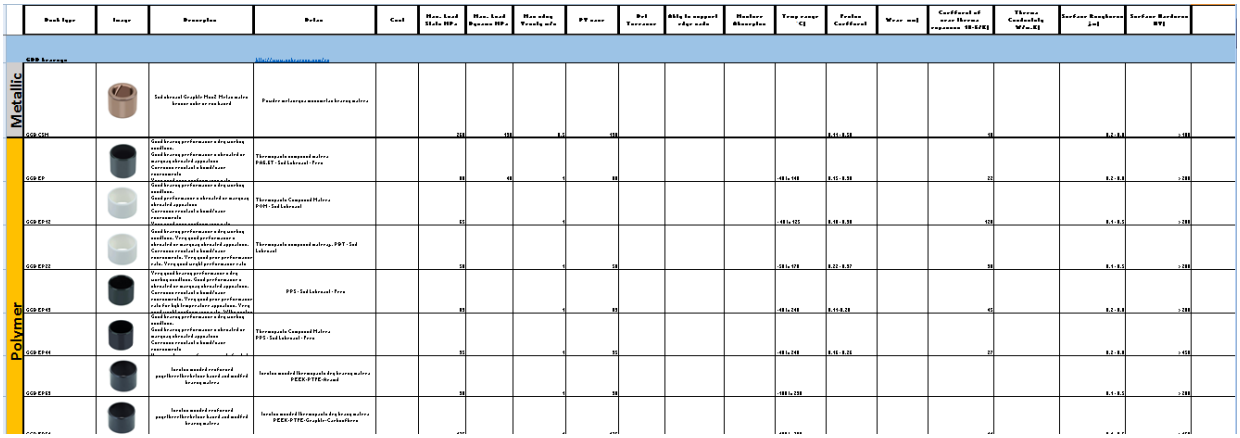

Figure 11.1.2: Part of the List of Self-Lubricating Bearings According to Company and Material Type and all their Found Properties

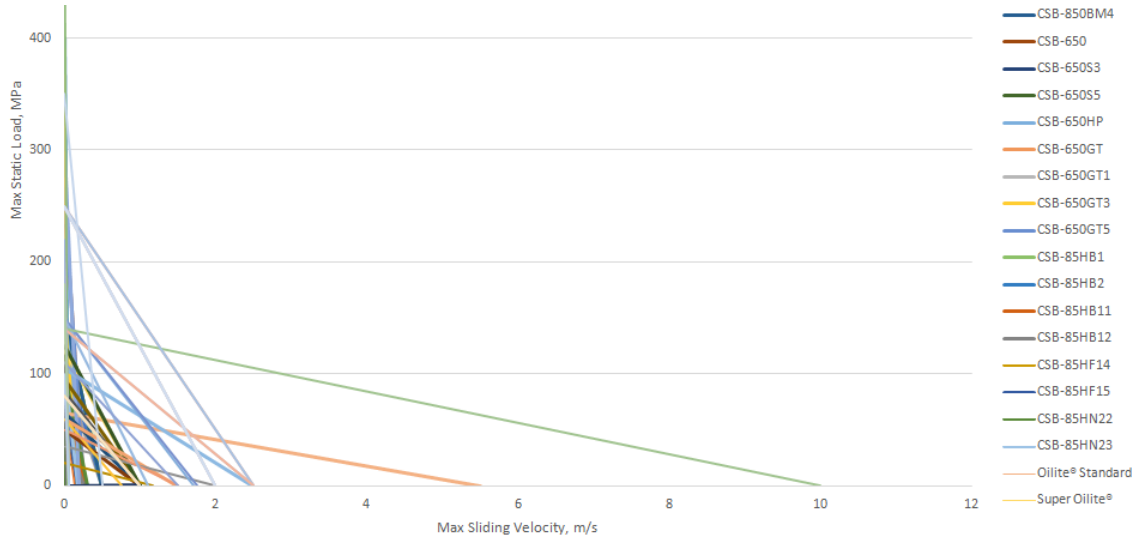

Figure 11.1.3: PV Chart

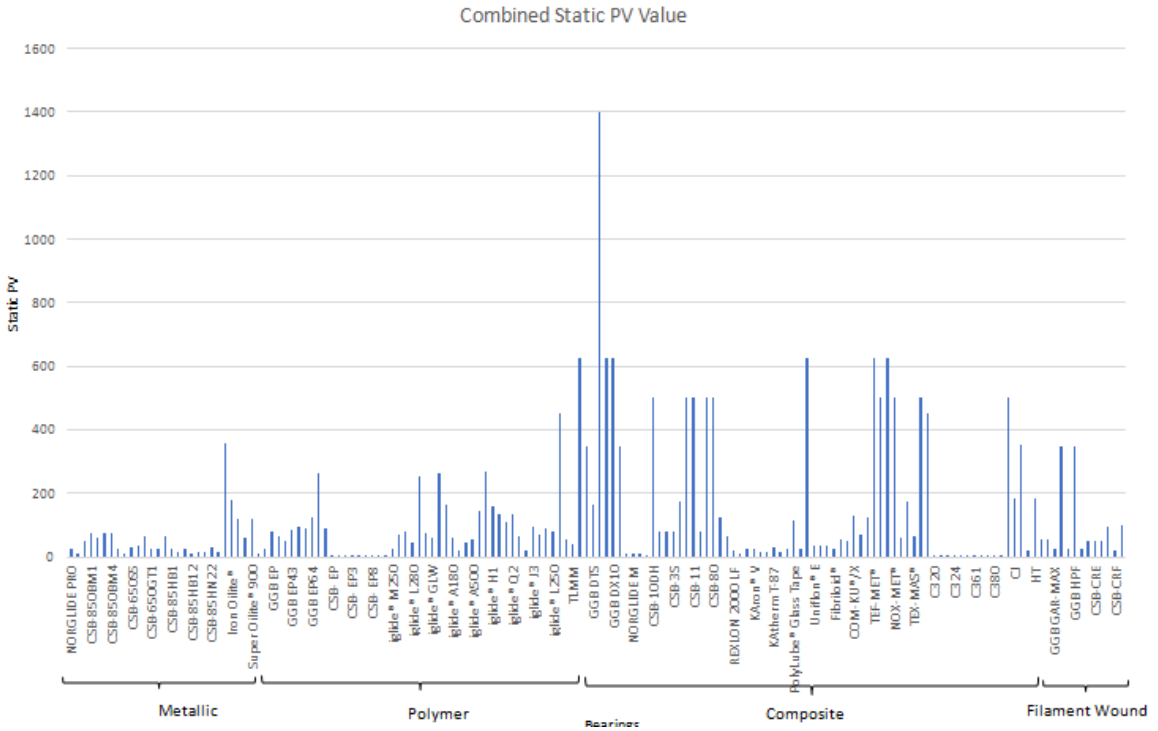

Figure 11.1.4: Combined PV Values

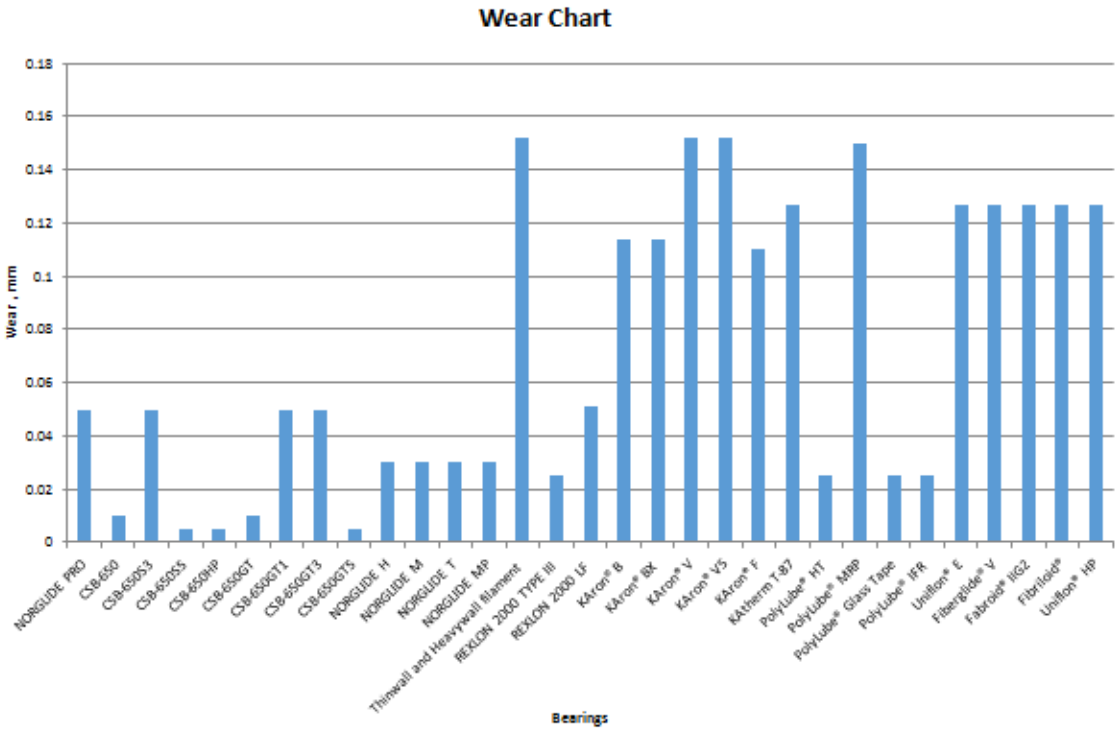

Figure 11.1.5: Wear Chart

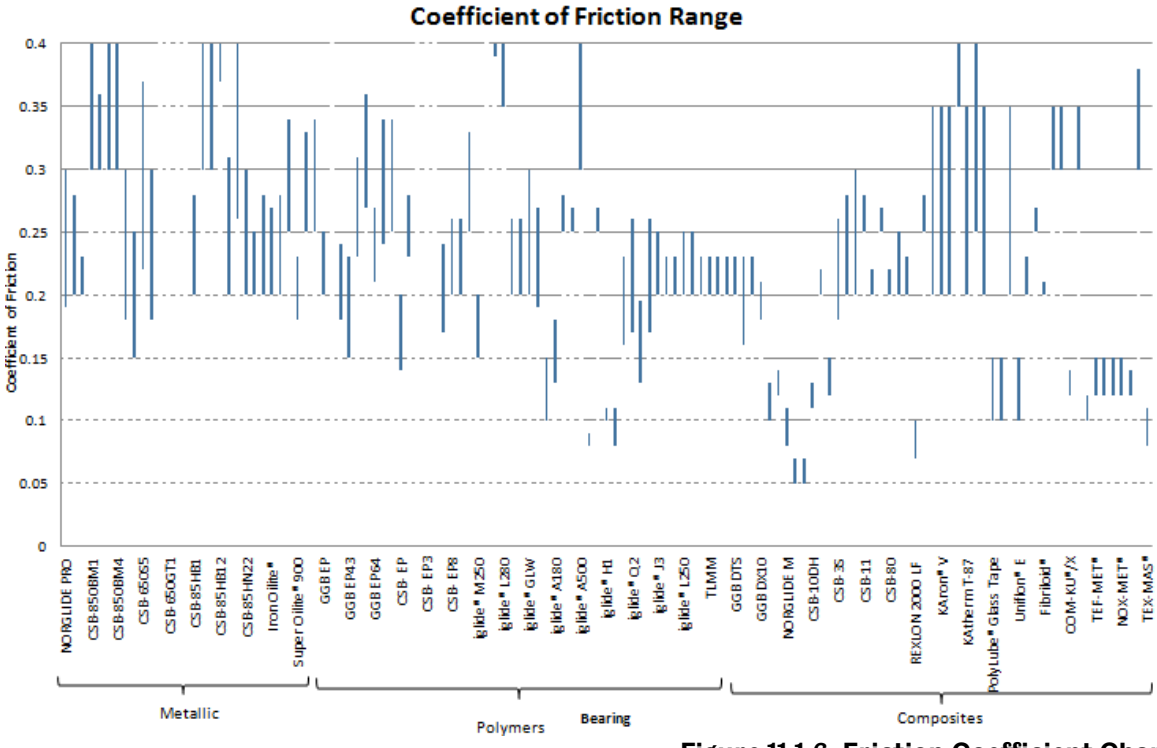

Figure 11.1.6: Friction Coefficient Chart

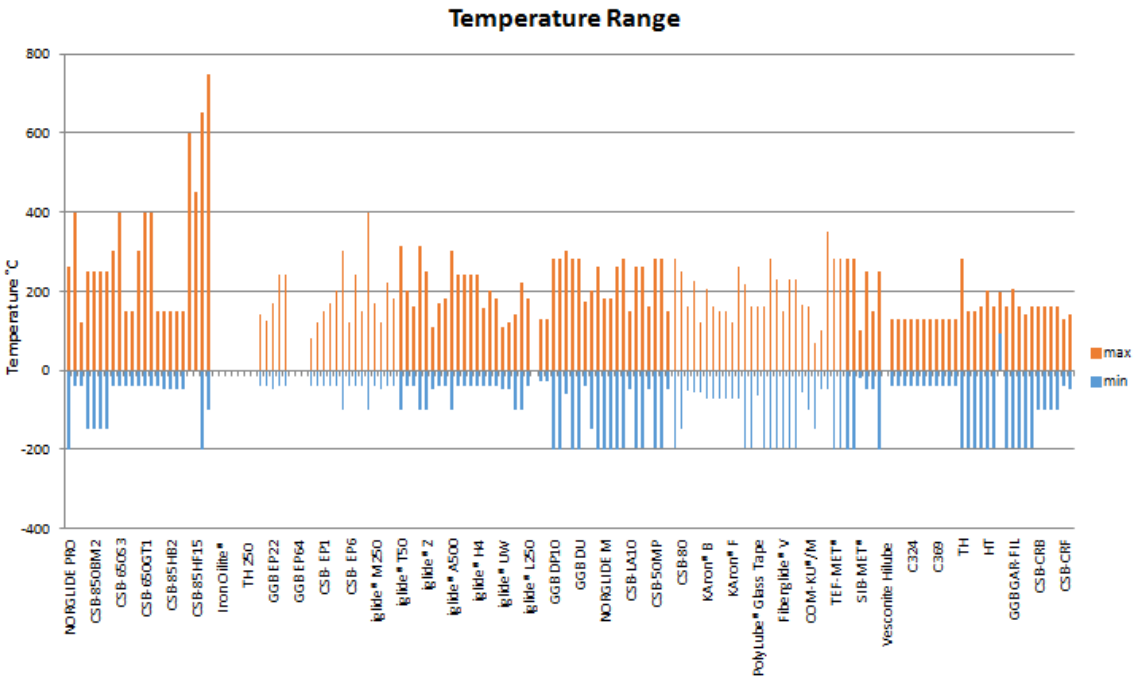

Figure 11.1.7: Temperature Range

11.2 **Appendix 2-Sizing Motor**

Calculations that were done to calculate the power needed for the shaft to rotate under 100MPa pressure. The bearing dimensions are: 25mm diameter and 10mm width.

$$P = \frac{F_P}{d \times w}$$

$$F_P = 100 \times 0.025 \times 0.01$$

$$F_P = 25000N$$

Using the maximum expected CoF of 0.4 torque can be calculated:

$$T = 0.04 \times 25000 \times 0.025$$

$$T = 125Nm$$

To calculate the power needed the rotational speed needs to be calculated first:

$$\omega = \frac{v}{2\pi r} = 136\frac{rad}{s}$$

$$P = T \times \omega = 125 \times 136 = 17kW$$

Motor Specifications:

- Manufacturer: SIEMENS
- Model number:1LC4 220-4AA5U
- 3-phase
- Voltage=440V
- Power output=37kW
- Maximum speed=1475rpm
- Frequency=50hz

11.3 **Appendix 3-Hydraulic Power Pack**

Model number= RCS 101

Cylinder capacity=101kN

Cylinder effective area=14.5cm^2

Oil capacity=55cm^3

Collapse Height=88mm

Extended height=126mm

Outside diameter=69mm

Weight=4.1kg

11.4 **Appendix 4-Torque transducer**

NAME	MIN	TYP	MAX	UNIT
CHANNEL 1				
Excitation (ꝑ)	5		11	Vdc
Hysteresis (ꝑ)	-0.1		0.1	% of R.O.
Input Resistance		350		Ohms nom.
Nonlinearity (ꝑ)	-0.2		0.2	% of R.O.
Nonrepeatability (ꝑ)	-0.2		0.2	% of R.O.
Operating Temperature (ꝑ)	41		122	F
Output Resistance		350		Ohms nom.
Rotational Speed	0		3000	RPM
Safe Overload (ꝑ)			150	% of R.O.
Temperature Shift Span (ꝑ)	-0.01		0.01	% of Load/F
Temperature Shift Zero (ꝑ)	-0.01		0.01	% of R.O./F
Zero Balance (ꝑ)	-1		1	% of R.O.
Capacity			500	N-m
Rated Output (ꝑ)		2		mV/V nom. (ꝑ)
Calibration Excitation		10		Vdc

11.5 **Appendix 5- Micro slip Model Proposal (Oloffson, 1997)**

Micro slip is commonly found within bearing systems, and can resulting in fretting on the joints. The sliding of surfaces against one another results in a deformation that occurs within the contact zone prior to a macro-slip occurrence. Ulf Olofsson defines micro slip as "a small tangential relative displacement in a contacting are at an interface, when the remaining area in the contact is not relatively displaced tangentially".

We adapted a micro-slip predictor, modelling the micro-slip between ellipsoidal bodies. This model held certain assumptions which was not supportive of our desired contact mode, which was a journal bearing in tension. However this model seemed to take into account necessary numerical values. The assumptions made were:

- Asperical shapes are ellipsoidal
- The height distribution of the asperities is uniform
- Individual asperities follow the hertzian theory for elliptical contact, while the surface contact remains elastic.
- Respectively, all the a and b axes have their semi-axes in the rightful and same x – direction and y-direction
- Asperities in contact have the same ovality ration, that is (a/b – constant)

Here, the asperities in contacts are to be further modelled as spheres, giving the cases where a = b, and ϕ=1. Also, the complete elliptical integral of the first and second kind is k = π/2. This in turn led to the frictional force being calculated as (Olofsson, 1997):

$$F = \mu P \left[1 - \left(1 - \frac{4G'\delta}{\mu E'\lambda} \right)^{\frac{5}{2}} \right]$$

We then rearranged the frictional force for δ (displacement, representing micro slip). The steps were as follows:

$$\frac{F}{\mu P} - 1 = -\left(1 - \frac{4G'\delta}{\mu E'\lambda} \right)^{\frac{5}{2}}$$

$$1 - \frac{F}{\mu P} = \left(1 - \frac{4G'\delta}{\mu E'\lambda} \right)^{\frac{5}{2}}$$

$$1 - \frac{F}{\mu P} = \left(\frac{\mu E'\lambda - 4G'\delta}{\mu E'\lambda} \right)^{\frac{5}{2}}$$

$$1 - \frac{F}{\mu P} = \left(\frac{1}{\mu E'\lambda} \right)^{\frac{5}{2}} (\mu E'\lambda - 4G'\delta)^{\frac{5}{2}}$$

$$\left(1 - \frac{F}{\mu P} \right) (\mu E'\lambda)^{\frac{5}{2}} = (\mu E'\lambda - 4G'\delta)^{\frac{5}{2}}$$

$$\left[\left(1 - \frac{F}{\mu P} \right) (\mu E'\lambda)^{\frac{5}{2}} \right]^{\frac{2}{5}} = \left[(\mu E'\lambda - 4G'\delta)^{\frac{5}{2}} \right]^{\frac{2}{5}}$$

$$\left(1 - \frac{F}{\mu P} \right)^{\frac{2}{5}} (\mu E'\lambda) = \mu E'\lambda - 4G'\delta$$

$$\left(1 - \frac{F}{\mu P} \right)^{\frac{2}{5}} (\mu E'\lambda) - \mu E'\lambda = -4G'\delta$$

$$\mu E'\lambda - \left(1 - \frac{F}{\mu P} \right)^{\frac{2}{5}} (\mu E'\lambda) = 4G'\delta$$

$$\mu E'\lambda \left[1 - \left(1 - \frac{F}{\mu P} \right)^{\frac{2}{5}} \right] = 4G'\delta$$

$$\frac{\mu E' \lambda \left[1 - \left(1 - \frac{F}{\mu P}\right)^{\frac{2}{5}}\right]}{4G'} = \delta$$

As our independent variable is the normal load (P), similar to the force that would be applied to a bearing material in the aircraft, and the coefficient of friction of the material is known, the friction force can be determined by the equation:

$$F = \mu P$$

G' and E' are determined by their respective equations taking into account the properties of the 2 materials interacting. Lambda (λ) is the normal difference in length between the smooth surface, and the centre line average of the rough surface, namely the specific film thickness. Because the bearings tested are used in dry rubbing, we will assume a concentric behaviour between the bearing and the bush. This allows us to calculate the normal separation between the journal and bearing using their radius.

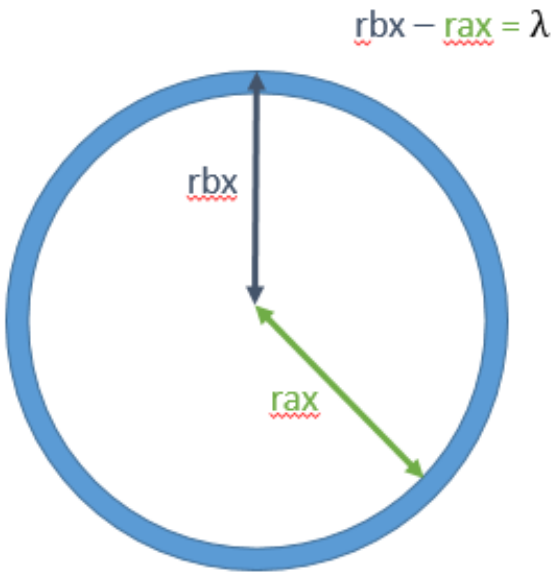

Figure 7.8.1: the radius of the journal and bearing. Not drawn accurately

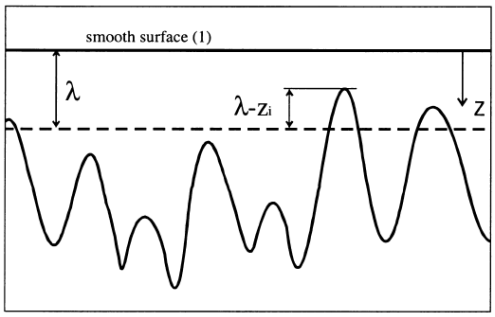

Figure 7.8.2: Close up two surfaces in contact. (Olofsson U, 1997)

The intent was for the frictional load, or normal load to be plotted against the displacement, as the normal and frictional loads will be directly proportional to one another and thus give a similar graph. Olofsson states that the displacement represents the micro slip zone, and is true up to maximum displacement, reached when product of the normal load and friction coefficient is equal to the frictional force.

$$F = \mu P$$

This means that when $\left[1-\left(1-\frac{F}{\mu P}\right)^{\frac{2}{5}}\right] > 1$ we will see sliding, and we will exceed the micro slip zone limit. Equating to find the maximum displacement allowed gives:

$$\frac{\mu E' \lambda \left[1-\left(1-\frac{F}{\mu P}\right)^{\frac{2}{5}}\right]}{4G'} = \delta$$

$$1-\left(1-\frac{F}{\mu P}\right)^{\frac{2}{5}} = 1$$

$$\left(1-\frac{F}{\mu P}\right)^{\frac{2}{5}} = 0$$

$$\frac{F}{\mu P} = 1$$

$$F = \mu P$$

This means that the maximum displacement allowed in the slip zone will equates to;

$$\frac{\mu E' \lambda}{4G'} = \delta_{max}$$

This wear model was not generated in the end and was neglected. Though we manipulated the model regarding parameters such as specific film thickness, this model was based on flat surface contacts, whereas we were looking for a more specified model that would account for both compression and tension loading, at specific points.